University of Texas Rio Grande Valley
ScholarWorks @ UTRGV

Theses and Dissertations

8-2020

Experimental Study of Graphene Energy Absorbing Layer in Femtosecond Infrared Laser Assisted Bioprinting

Chaoran Dou
The University of Texas Rio Grande Valley

Follow this and additional works at: https://scholarworks.utrgv.edu/etd

 Part of the Manufacturing Commons

Recommended Citation

Dou, Chaoran, "Experimental Study of Graphene Energy Absorbing Layer in Femtosecond Infrared Laser Assisted Bioprinting" (2020). *Theses and Dissertations*. 656.
https://scholarworks.utrgv.edu/etd/656

This Thesis is brought to you for free and open access by ScholarWorks @ UTRGV. It has been accepted for inclusion in Theses and Dissertations by an authorized administrator of ScholarWorks @ UTRGV. For more information, please contact justin.white@utrgv.edu, william.flores01@utrgv.edu.

EXPERIMENTAL STUDY OF GRAPHENE ENERGY ABSORBING LAYER IN FEMTOSECOND INFRARED LASER ASSISTED BIOPRINTING

A Thesis

by

CHAORAN DOU

Submitted to the Graduate College of
The University of Texas Rio Grande Valley
In partial fulfillment of the requirements for the degree of

MASTER OF SCIENCE IN ENGINEERING

Aug 2020

Major Subject: Manufacturing Engineering

EXPERIMENTAL STUDY OF GRAPHENE ENERGY ABSORBING LAYER IN FEMTOSECOND INFRARED LASER ASSISTED BIOPRINTING

A Thesis
by
CHAORAN DOU

COMMITTEE MEMBERS

Dr. Jianzhi Li
Chair of Committee

Dr. Ben Xu
Committee Member

Dr. Andrew Tsin
Committee Member

Dr. Zhenyu Kong
Committee Member

Aug 2020

Copyright 2020 Chaoran Dou
All Rights Reserved

ABSTRACT

Dou, Chaoran, Experimental Study of Graphene Energy Absorbing Layer in Femtosecond Infrared Laser Assisted Bioprinting. Master of Science in Engineering (MSE), Aug, 2020, 89 pp., 4 tables, 60 figures, 51 references, 31 titles.

The bioprinting, as a new branch of additive manufacturing, already shown its potential in organ transplantation, medicine develop and personalized medicine. There are three types of bioprinting: droplet based bioprinting, extrusion based bioprinting and laser assisted bioprinting (LAB). Compared with other types of bioprinting, the LAB is the only bioprinting method that does not have a nozzle, which gives it the ability to print high viscosity bioink. The LAB also enjoys higher resolution and cell viability than other methods.

The bubble/jet formation process is the most important process for the LAB, which deposits the bioink to the substrate. To utilize laser energy, the energy absorbing layer (EAL) is essential to the printing process. This study explored graphene as a new material for the EAL and tested its energy absorbing performance under a controlled environment. This thesis also proved that the higher laser pulse deposits a higher volume of bioink.

DEDICATION

To my Mom and Dad

Your love is the foundation of my happiness

To my Grandaunt

Your waiting is the beacon of my life

To my Friends

To our laughter and tears in the past and future

LOVE YOU

CHEERS

ACKNOWLEDGMENTS

I am immensely thankful to Dr. Jianzhi Li, chair of my thesis committee, for all his mentoring, support and advice. From the beginning of this study, he guided me with a great level of the profession and infinite patience. I wholeheartedly thank my thesis committee members: Dr. Andrew Tsin, Dr. Ben Xu and Dr. Zhenyu Kong. Their advice, input, and comments on my thesis helped to ensure the quality of my intellectual work. I also want to express my deepest gratitude to the University of Texas Rio Grande Valley and the manufacturing engineering department for allowing me to conduct my research and providing any assistance requested. I also give a special thanks to associates from our lab, especially Jie Qu, for all the time we spent working together.

TABLE OF CONTENT

Page

LIST OF TABLES

Page

LIST OF FIGURES

Page

CHAPTER I

INTRODUCTION

1.1 Background

By accelerating the transmission of information, printing technology is undoubtedly recognized as one of the most essential inventions in human history. Nowadays, driven by the rise of modern information science and the popularizing of electronic media terminals, electronic screen replaced paper, become the new favorite of the information industry. However, this is not the end of the printing technology, from the 2D plane to the 3D solid, 3D printing or additive manufacturing evolved from traditional 2D printing, which opens a new area for the history of printing. Stand at the frontier of the future science, 3D printing is not only described as a vehicle of information, but it is also carrying the hope of future manufacturing industry, future medical industry, or even expected as a trigger of the fourth industrial revolution.

Bioprinting, as a new branch of additive manufacturing, different from metal or ceramic based technology, has a greater ambition in changing human lives. Welcomed by the medical industry, bioprinting shows its potential in many aspects of medical usage such as personalized medicine, organ transplant, drug development, etc.

1.2 Laser assisted bioprinting

Based on a technology invented in 1986 which called laser induced forward transfer (LIFT)(Bohandy et al. 1986), the laser assisted bioprinting appears in 2004(Barron et al. 2004c; Barron et al. 2004b; Fernández-Pradas et al. 2004). As a revolutionary bioprinting technology, the LAB brings high resolution and high cell viability to the bioprinting realm. It can achieve the resolution as high as few microns and it has the potential to achieve 100% cell viability, both are the highest among all bioprinting technology(Barron et al. 2004c; Barron et al. 2004b; Fernández-Pradas et al. 2004).

The LAB printer is composed of three major modules, they are the laser generator, the optical adjusting mirrors, and the bioink transfer module. The bioink transfer module has a ribbon which is usually made of transparent quartz or glass which absorbs the laser power as less as possible and provides enough support for the bioink layer. The substrate is another component of the bioink transfer module. Just like the ribbon, the substrate is also made of transparent glass or quartz.

The ribbon is usually coated with a thin layer of laser absorbing material and this coated layer is called energy absorbing layer or laser absorbing layer. Beneath the energy absorbing layer, the bioink layer is coated. The bioink is the biomaterial that needs to be transferred to the receiving substrate.

The substrate is installed under the ribbon with a small gap like a few hundreds of microns. In some cases, there is a thin layer of liquid or gel is applied on the upper surface of the substrate to protect the falling biomaterials.

There are five steps for the laser assisted bioprinting, they are:

First, the laser pulse is emitted by the laser generator, and the light path is guided by mirrors towards the designed position.

Second, the laser beam is focused on the upper surface of the energy absorbing layer by the focusing lens.

Third, the laser energy is absorbed by the EAL and the EAL is vaporized. A bubble is generated in the bioink layer.

Forth, the expansion of the vapor bubble pushes the bioink and generates a jet.

Finally, the jet lands on the substrate and the bioink is transferred.

Different from other bioprinting methods, the LAB has a unique setup and uses a laser generator as the energy source. Many parameters can be controlled in the printing process like laser pulse energy, laser spot size, the thickness of the bioink layer, etc. The unique mechanism of the LAB bioprinter and operating process give it several unique features, they are:

Advantages

1. The LAB enjoys high accuracy and high-resolution in biomaterial deposition. The micron level resolution provides LAB the capacity in locating microdroplets in a designed position or isolating single cells/cell aggregation (Cheptsov et al. 2018).
2. The printing throughput is controlled by the laser pulse frequency. When equipped with a high-frequency laser generator, the LAB can achieve high throughput printing (Guillotin et al. 2010).
3. The LAB is a bioprinting technology with nozzle-free structure, instead of storing the bioink in a container, it is coated on a quartz plate, which ensures the LAB can print without clogging while using high viscous bioink or cell-laden bioink (Guillemot et al. 2010b, Delaporte and Alloncle 2016).

4. As reported in the literature, the cell viability of LAB is much higher than other types of bioprinting. Usually, the viability is higher than 80% and can achieve 100% cell viability in some cases (Fernández-Pradas et al. 2004).

Disadvantages

1. The build cost of the LAB printer is higher than other types of bioprinter.
2. The complex procedure of printing affects the overall efficiency.
3. The types of cells that can be processed is limited.

1.3 Research problem

To have a better understanding of the LAB process, the objective of this thesis is to study the parameters which will affect the performance of LAB especially the bubble/jet formation process. Finding an EAL material that both has high laser energy absorbing rate and cause less damage to the bioink or cells is another research topic of this study.

To investigate the printing process of the LAB to provide answer to the following questions:

1. What is the fundamental physics in bubble/jet formation in LAB;
2. Graphene has been tested as biocompatible in a few studies (Pinto et al. 2013), can graphene be used as an energy absorbing layer material;
3. What is the best thickness for the energy absorbing layer;
4. What are the effects of different laser energy on the bubble formation?

1.4 Organization of the thesis

This thesis is organized as follows: Chapter one introduction discusses the invention of the LAB, its significance, and the problems faced. The objectives and plan are also given in chapter one; Chapter two reviews the most recent research literature regarding three different research topics of the LAB, they are 1. Different designs of the LAB printer; 2. Development in the EAL; 3. Research on bubble/jet formation. In Chapter III, the structure of the LAB printer used in the experiments is introduced and the experimental protocol is designed. This includes the parameters chosen, the value of the parameters and preparation work. Chapter IV shows the experiment samples and discussed the results. Chapter V summarizes the work in the thesis and provides a future plan.

CHAPTER II

LITERATURE REVIEW

2.1 LAB process setup

The LAB bioprinter is a complex system, as shown in Figure 1. Three main modules parts make the whole system function, they are laser system, mirror/lens system, and printing module. Those modules should cooperate to print the bioink on the designed location.

Laser system

The laser is the only energy source in the LAB printer which plays an important role in bubble/ jet formation. There are many different types of laser has been tested in the LAB such as excimer laser(Ringeisen et al. 2014), Nd: YAG laser(Keriquel et al. 2017; Kerouredan et al. 2019; Serra et al. 2009; Gruene et al. 2011a; Fernández-Pradas et al. 2007), ruby laser(Nguyen and Narayan 2017), etc. Those lasers can also be classified by its wavelength from 94nm to 1064nm(Nguyen and Narayan 2017)(Othon et al. 2008)(Chen et al. 2006)(Serra et al. 2009; Fernández-Pradas et al. 2007)(Keriquel et al. 2017; Gruene et al. 2011a). It is believed that the long wavelength IR laser will cause less damage to the biomaterial because the short wavelength laser can kill the cells by breaking the DNA double strand and the membrane (Guillemot et al. 2010b; Pagès et al. 2015)(Zhang et al. 2018). Among all laser systems, the nanosecond laser is the most wildly used. At the same time, some short pulse duration such as picosecond laser and

Femtosecond (Duocastella et al. 2010a; Dinca et al. 2008)(Zergioti et al. 2005; Karaiskou et al. 2003) are also tested. It is believed that the longer the pulse duration is, the more heat effect the laser will brings to the bioink, consequently, the cells especially those heat sensitive cells in the bioink will suffer from more heat damage (Hopp et al. 2010).

Mirror/lens system

The mirror and lens system are composed of mirrors and lenses to adjust the light path of the laser and locate the focal point at the printing location. The mirrors reflect the laser beam to adjust its direction and the lens enlarges or focuses the laser beam.

Printing module

The printing module consists of a transparent ribbon, an energy absorbing layer, bioink layer, and a receiving substrate. The ribbon and the substrate are made of transparent materials such as glass or quartz. The ribbon is to provide a solid support for the energy absorbing layer and the bioink layer. The substrate is to provide a landing environment for the jet and droplet. The EAL is a very thin layer designed to absorb the laser energy and convert it to the kinetic energy of the bioink. The EAL is the key feature to distinguish the absorbing layer assisted LIFT (AFA-LIFT) and the matrix assisted pulse laser evaporation direct writing (MAPLE-DW). Different from the AFA-LIFT, the MAPLE-DW utilizes the bioink itself instead of EAL as the laser absorbing medium.

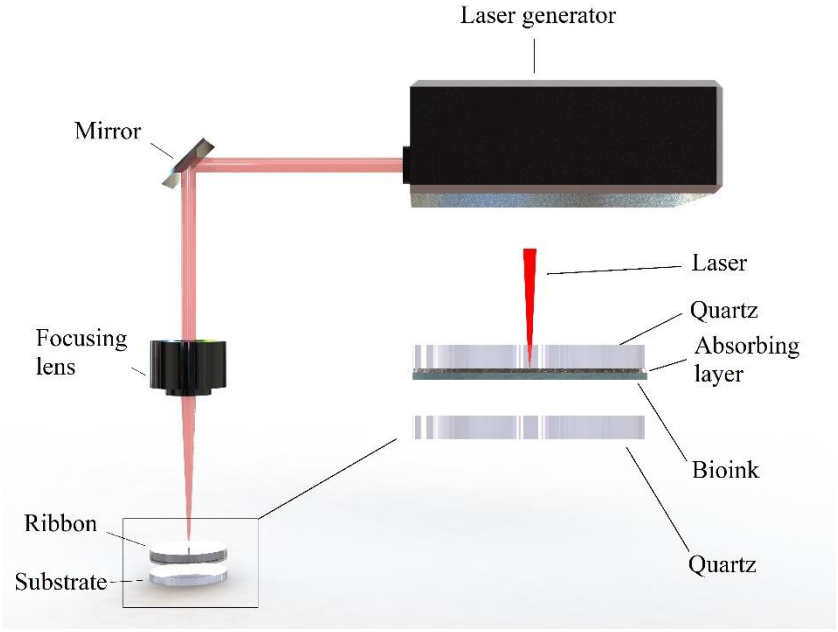

Figure 1: The structure and main components of laser assisted bioprinter

There are five steps for LAB to print a drop of bioink on the substrate(Serra et al. 2009; Duocastella et al. 2010b; Duocastella et al. 2009; Unger et al. 2010; Duocastella et al. 2008; Guillemot et al. 2010a)

First, the laser pulse is irradiated by the laser generator, and the light path is guided by mirrors towards the designed position.

Second, the laser beam is focused on the upper surface of the energy absorbing layer by the focusing lens.

Third, the bubble starts to be generated, at the beginning of the bubble generation, the bubble inner pressure is higher than the surrounding pressure. Driven by the pressure difference, the bubble expands very rapidly and pushes the liquid downwards.

Fourth, with the releasing of pressure by expansion, the inner pressure is gradually equal to the outside pressure, at this time, the bubble keeps expanding due to the inertia of the material. At this stage, the bubble can have a short time of oscillation.

Fifth, the bubble pressure is lower than the liquid pressure, at this longer stage, the bubble starts to shrink and collapse, which is followed by the formation of the jet.

2.2 The absorbing layer

The energy absorbing layer (EAL) is a thin layer attached to the bottom of the transparent ribbon. It is an impotent but not indispensable part of the cell transfer module. By using the EAL layer or not, two different types of LAB are distinguished, they are absorbing layer assisted LIFT (AFA-LIFT)(Hopp et al. 2004; Hopp et al. 2005) and the matrix assisted pulse laser evaporation direct writing (MAPLE-DW)(Barron et al. 2004a).

The EAL, just like its name, is a specially designed layer to absorb the energy from the laser pulse. It has a higher laser absorbing rate than the bioink(Hopp et al. 2010; Doraiswamy et al. 2006). It also isolates the laser radiation and the biomaterial physically, which protects the cells from laser damage(Doraiswamy et al. 2006; Smausz et al. 2006). It was proved(Catros et al. 2011) that almost all energy is absorbed by bioink and cells are damaged if there is no EAL present. The EAL can also help to smooth the jet formation process.

However, it is not always an advantage to have an EAL. When absorbing the laser energy, the EAL will be broke in some cases, as shown in Figure 2 (Deng et al. 2017). In this case, the EAL is not reusable and must be recoated after printing, which slows down the printing speed. When the EAL is broken, the fragments of EAL will disperse in the bioink and become a potential risk to contaminate the bioink and damage the cells(Brown et al. 2010; Lin et al. 2011).

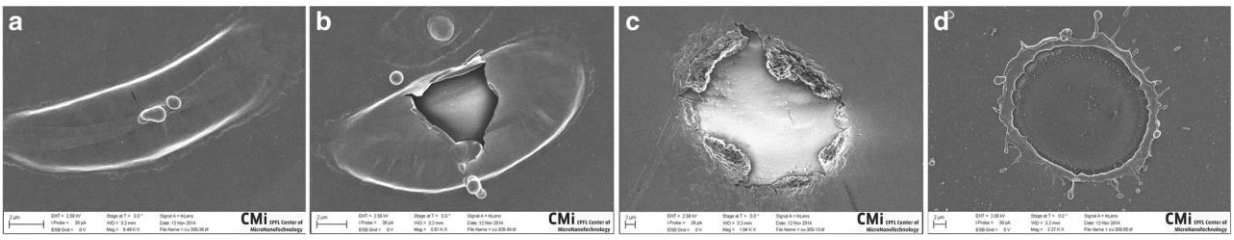

Figure 2: The morphologies of titanium layer after LIFT process (Deng et al. 2017)

Traditional EAL materials are metal and metal oxides, such as Ti(Koch et al. 2014), titanium oxide(Othon et al. 2008; Haider et al. 2017), Gold(Koch et al. 2018), Silver(Smausz et al. 2006) and polyimide(Brown et al. 2010).

To protect the biomaterial, the thickness of the EAL should larger than the penetration depth of the EAL material under the laser used(Serra and Piqué 2019). The EAL thickness can be so different for different materials, for example, the metal EAL usually has a thickness at 10-100nm, which is much thinner than the 500-1000nm of polymer EAL should be(Lin et al. 2011; Chen et al. 2006; Guillemot et al. 2010a).

From the previous paragraphs, a conclusion can be made that a nicely designed EAL not only can absorb the laser effectively and protect the biomaterial but also generate fewer fragments. To achieve this goal, various attempts have been made by researchers.

Lin et al. (Lin et al. 2011) designed a two-layer EAL, which consists of an adhesive layer and a metallic foil layer. As shown in Figure 3 the adhesive layer is applied to glue the metallic foil on the ribbon. Compared with the MAPLE-DW, this EAL design has a slower jet speed and a higher cell viability. The metallic foil will not break after the printing.

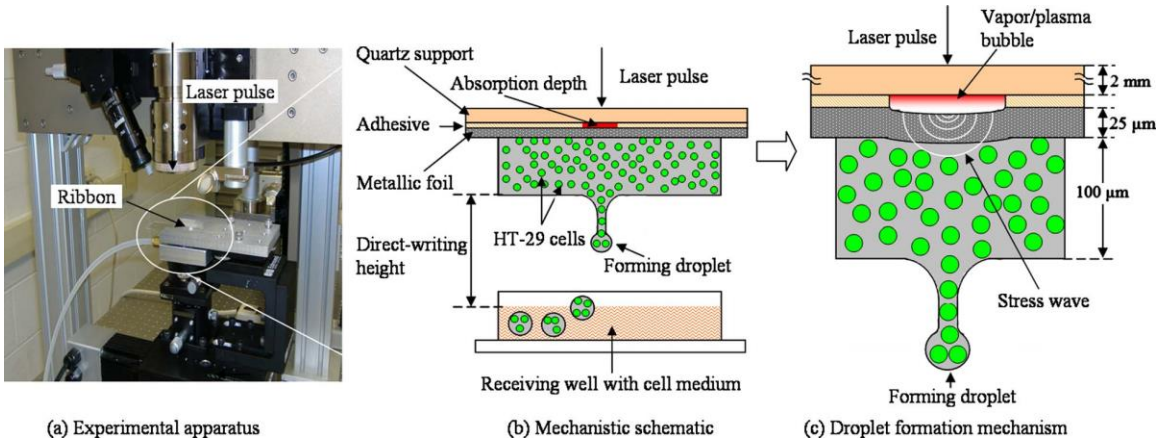

Figure 3: Metallic foil-assisted laser assisted bioprinting (Lin et al. 2011)

Xiong et al. (Xiong et al. 2017) tested the gelatin as the EAL material. The laser absorbing rate of the gelatin is better than the bioink, which allows the same size of jet or droplet with lower laser energy. Lower laser energy means higher cell viability. As shown in Figure 4. the viability was 10% higher when compared with no EAL, and the DNA damage was half as no EAL.

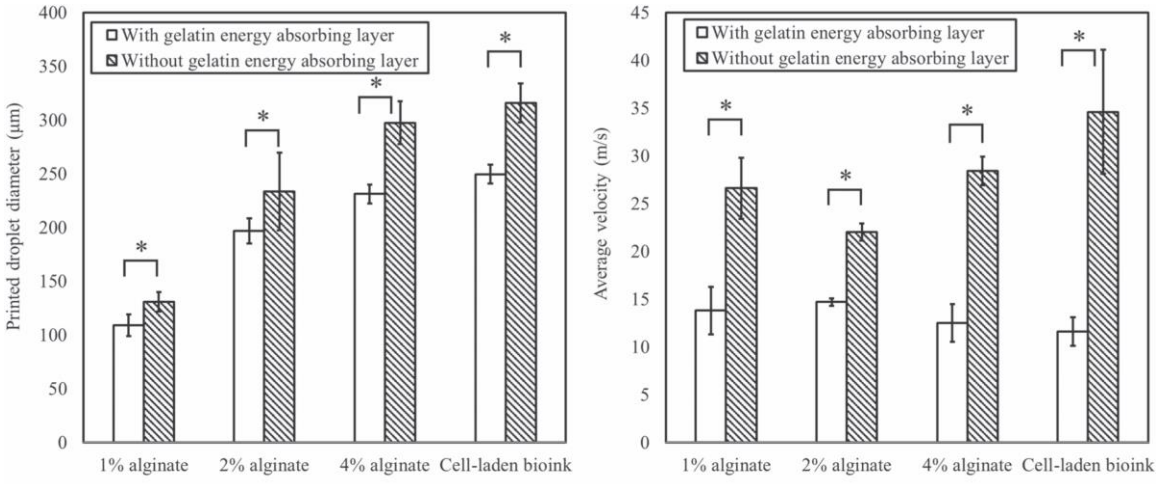

Figure 4: (a) Deposited droplet size and (b) average jet velocity with and without the gelatin EAL (Xiong et al. 2017)

By using traditional EAL material, the break of the EAL layer after printing is almost inevitable, which requires recoating of the EAL after each printing. This additional step slows down the printing process. To solve this problem, a reusable EAL is needed. Poly (dimethylsiloxane), PDMS, and other ceramics are tested for this purpose (Charipar et al. 2019).

2.3 Parameters

The value of the parameters is related to the performance of the LAB bioprinting. Those parameters are Laser pulse energy, Laser spot size, the thickness of the absorbing layer, the thickness of the bioink layer, travel distance, and the properties of the bioink. With different values of those parameters, the printing performance like bubble generation, jet size, droplet size, travel speed, and cell viability will be different (Deng et al. 2017; Yan et al. 2013; Gudapati et al. 2014; Guillemot et al. 2010a).

There are three different morphology of the bubble/jet formation by applying different laser pulse energy(Guillemot et al. 2010b; Duocastella et al. 2009; Guillotin et al. 2013). As shown in Figure 5. When the laser pulse energy is low, the bubble formation will be in the subthreshold regime, which means the bubble expansion is not strong enough to form a jet and deposit bioink on the substrate. When the laser passes the threshold, the bubble expansion will lead to the jetting of bioink. If the laser pulse energy is too high, the bubble will break and the plume will appear, which is not good for printing (Duocastella et al. 2007; Duocastella et al. 2008a) (Guillemot et al. 2010a) (Zhang et al. 2015).

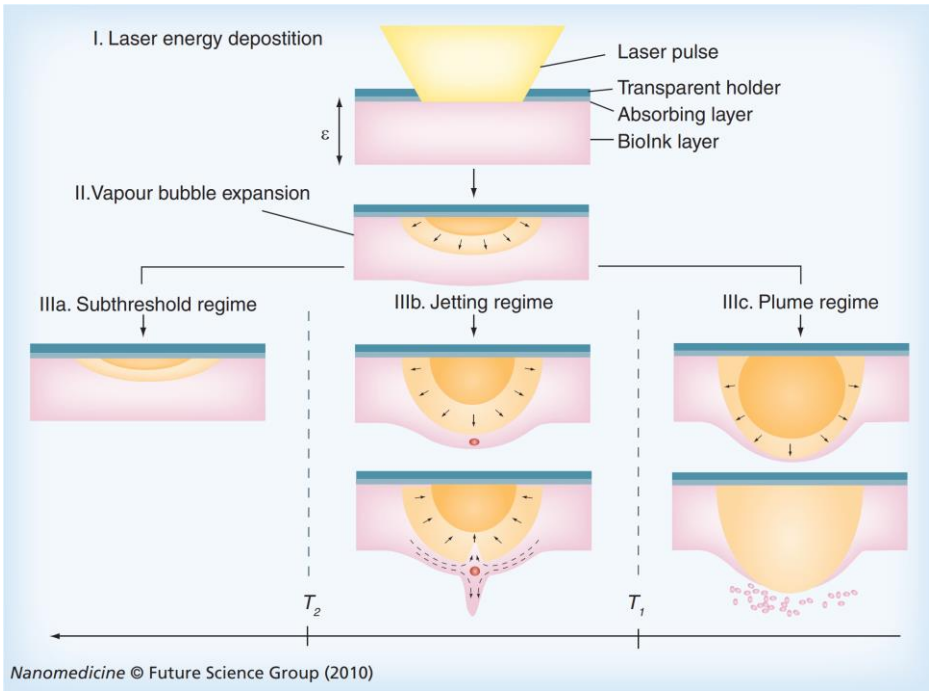

Figure 5: Three regimes for laser assisted bioprinting (Guillemot et al. 2010a)

As shown in Figure 6 and Figure 7, when the laser pulse energy goes higher, the volume of the bioink droplet also goes higher. Many researchers reported that the volume of deposited bioink is liner related with the laser pulse energy(Guillotin et al. 2010; Catros et al. 2011; Serra et al. 2009; Gruene et al. 2011b; Fernández-Pradas et al. 2007).

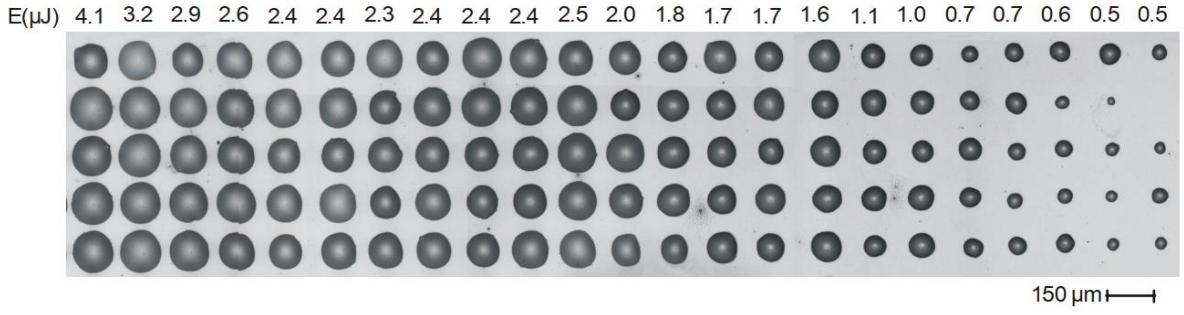

Figure 6: Droplets transferred at different energies (Fernández-Pradas et al. 2007)

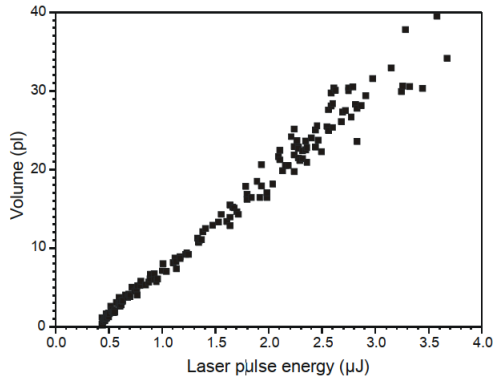

Figure 7: Transferred droplet volume versus laser pulse energy (Fernández-Pradas et al. 2007)

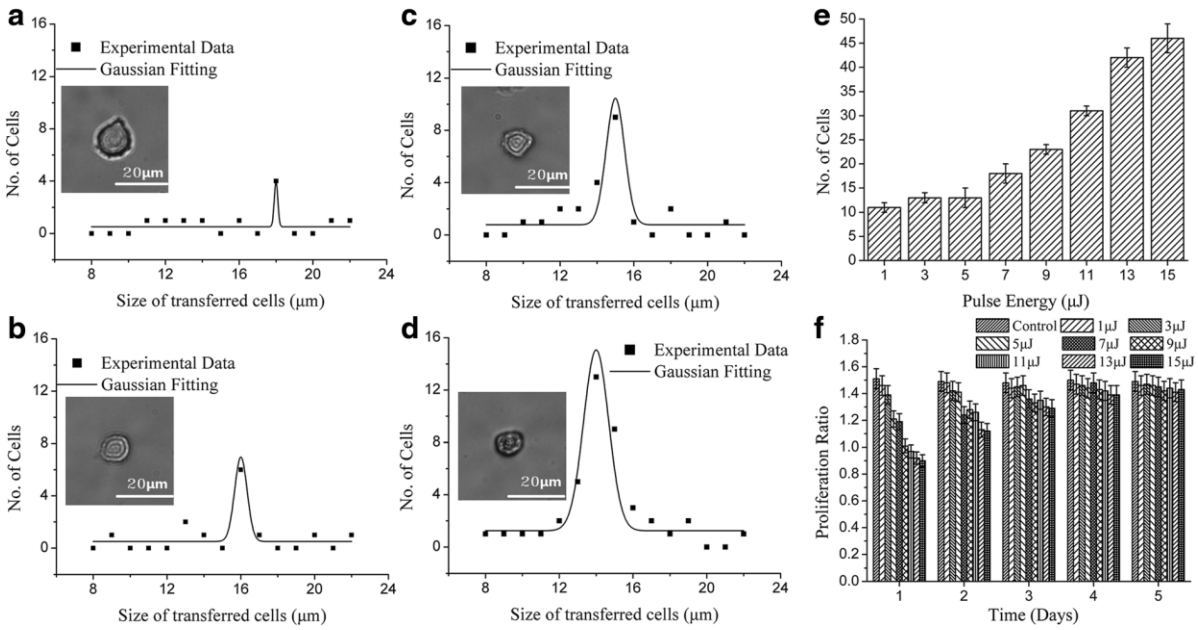

Figure 8 The impact of laser pulse energy (Deng et al. 2017)

The bioink viscosity is another essential parameter to the LAB bioprinting(Zhang et al. 2016; Yan et al. 2013). Bioink with higher viscosity has a higher threshold of laser pulse energy for the jet formation and less spreading and plume effect when landing on the substrate. Yan et

al. (Yan et al. 2013) also reported that low viscosity is not good for structure printing and low viscosity reduces the printing resolution.

With the same laser pulse energy, the smaller laser spot size is, the higher laser fluence will be. High resolution is easier to achieve when the laser spot size is small. However, a larger laser spot size with lower laser fluence can produce fewer EAL fragments (Brown et al. 2010).

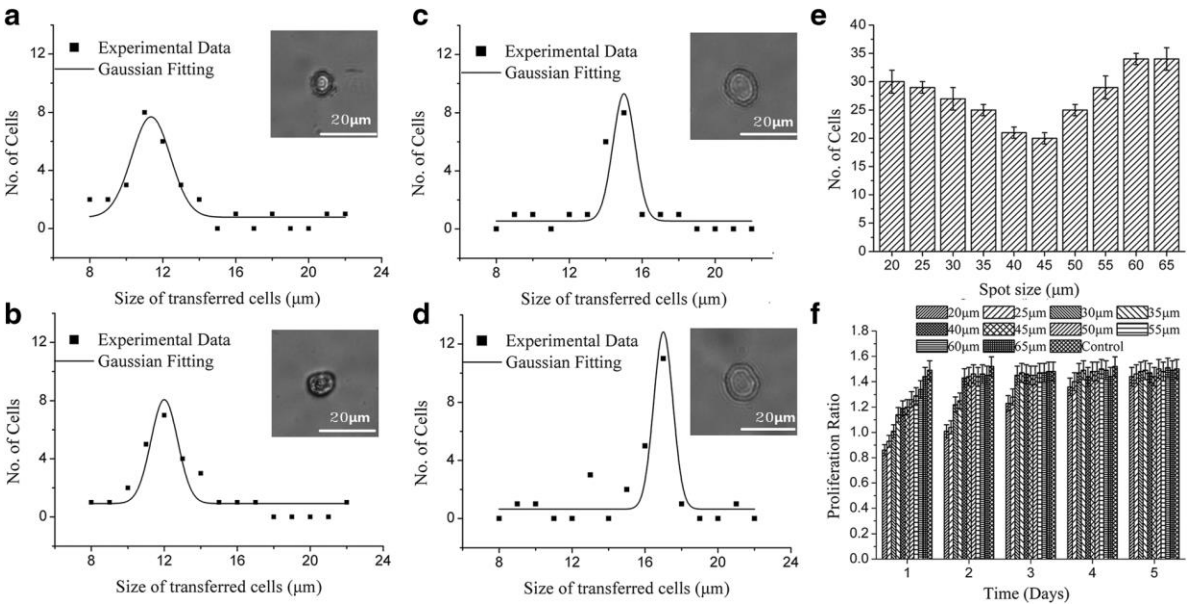

Figure 9: The impact of spot size (Deng et al. 2017)

The distance between the bioink layer and the receiving substrate is named travel distance, which ensures the bubble and jet have enough space to develop. When the distance is shorter than the threshold for the jet to fully develop, the number of cells deposited on the substrate will be unstable(Deng et al. 2017). As shown in Figure 10, when the distance is greater than 500μm, the jet is fully developed, and the number of deposited cells is stable.

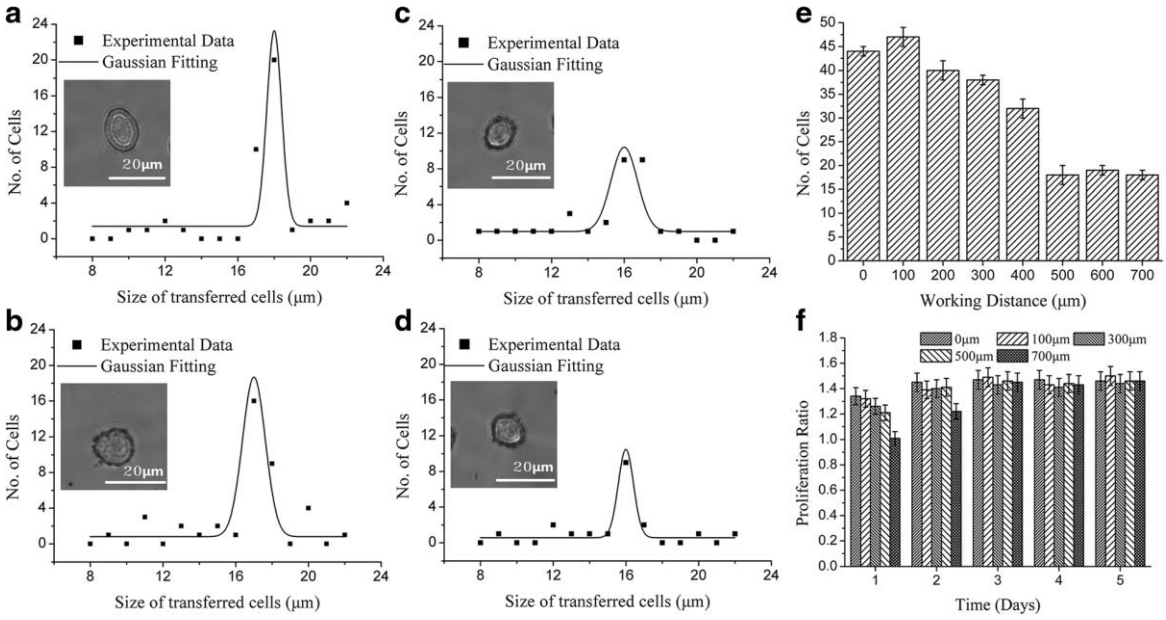

Figure 10: The impact of transfer distance (Deng et al. 2017)

As the most essential component, the cell plays an important role in the LAB printing, which will change the printability of bioink. Compared with bioink without cells, the bioink with cells has a higher printing threshold for laser pulse energy. Due to its inhomogeneity, the non-straight jet may show up, as shown in Figure 11(Zhang et al. 2017).

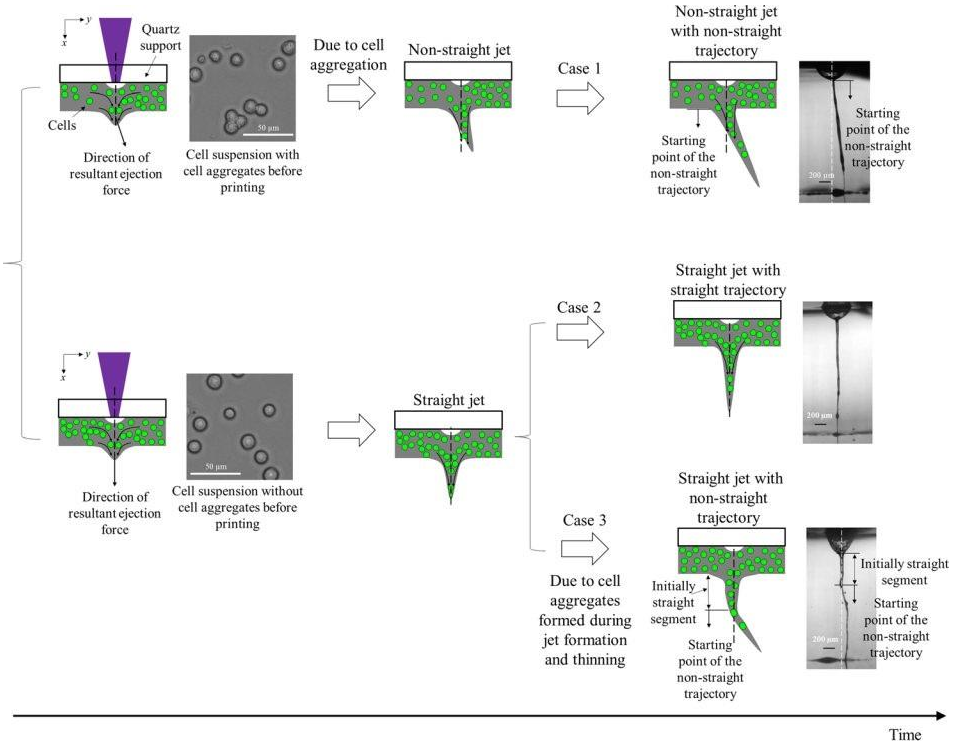

Figure 11: Schematics illustrating the formation of different types of jets during the laser printing of the cell-laden bioink (Zhang et al. 2017)

2.4 Bubble/jet formation

When the laser hits on the EAL, the bubble/jet formation process is triggered by the laser energy. By controlling the bubble/jet formation process, the printing result can be optimized. However, the physics of the bubble/jet formation has not been fully explored (Unger et al. 2010).

Many researchers reported that it is the bubble expansion that controls the jet formation and jet morphology. (Guillemot et al. 2010b; Brown et al. 2010; Unger et al. 2010; Guillotin et al. 2013; Mezel et al. 2010). The bubble/jet formation process is shown in Figs. 12, 13, and 14. There are three steps for bubble formation (Brown et al. 2010; Unger et al. 2010; Mezel et al. 2010):

1. When the laser energy is absorbed by the EAL, in the initial bubble, the pressure is higher than the pressure in the bioink. In this step, the bubble expands very quickly.
2. After the rapid expansion, the pressure in the bubble equals the pressure in the bioink, the bubble will expand slowly due to inertia and oscillation will appear(Brown et al. 2010).
3. After the bubble expands to its maximum size, the pressure inside of the bubble is lower than outside. At this step, the bubble starts to collapse and the jet is generated.

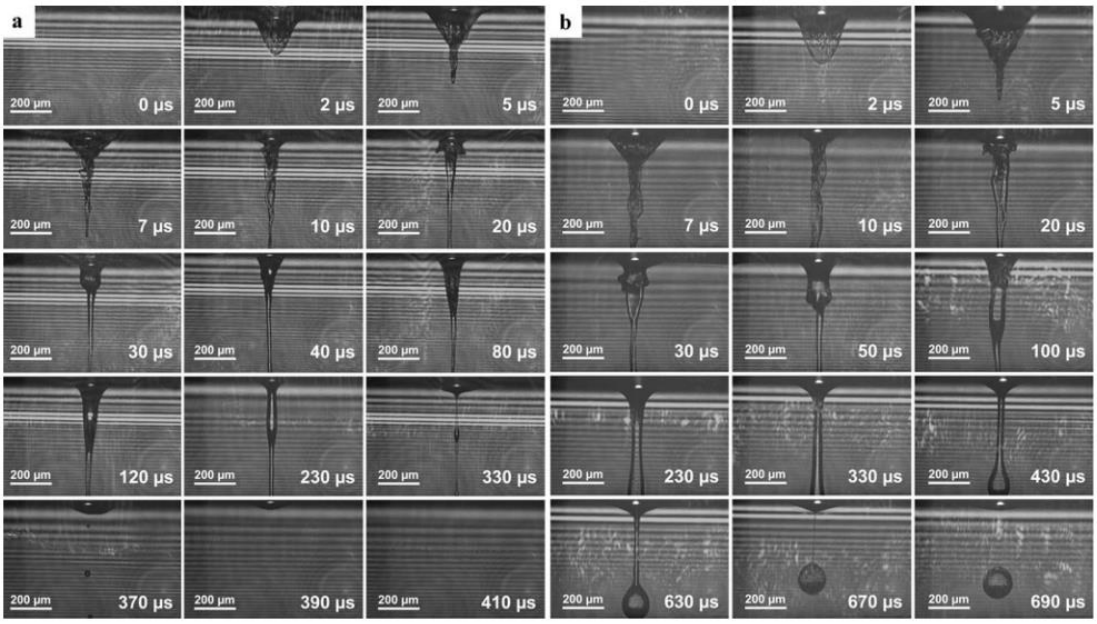

Figure 12: Time-resolved images of the hydrogel jet formation during LIFT without substrate at a laser fluence of (a) 1.6 J/cm2 and (b) 2.7 J/cm2(Unger et al. 2010)

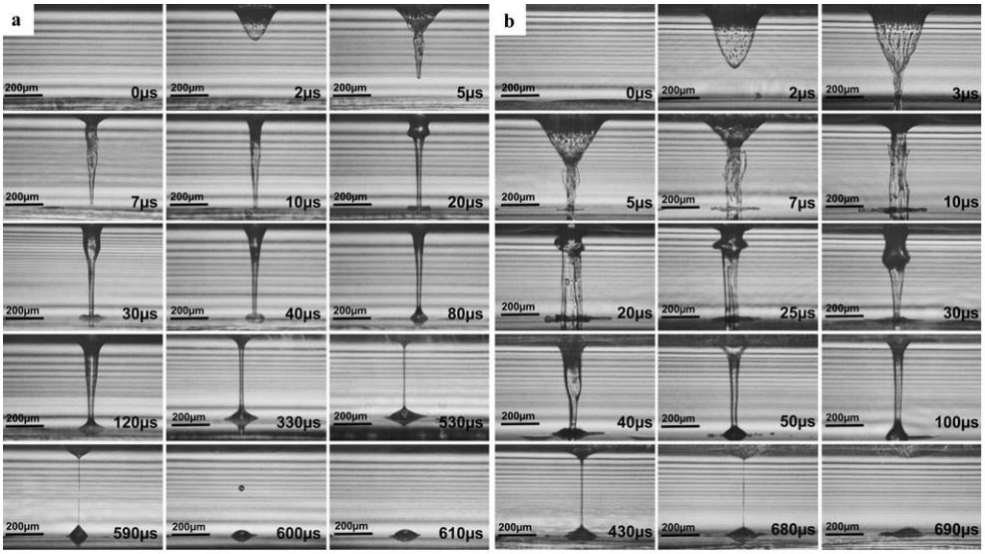

Figure 13: Time-resolved images of the hydrogel-transfer on the substrate via LIFT. The laser fluence initiating LIFT is (a) 1.6 J/cm2 and (b) 2.7 J/cm2. The gap between the donor and substrate is around 450 µm (Unger et al. 2010)

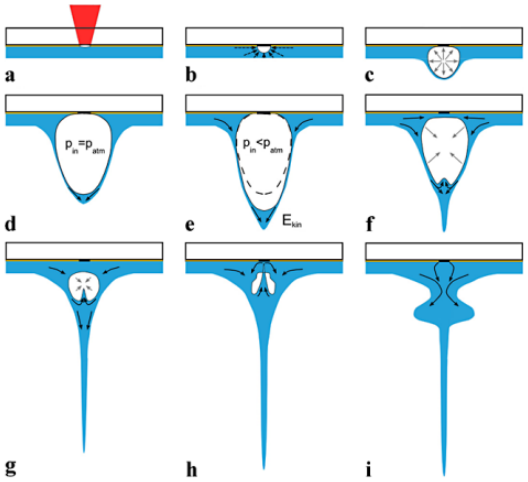

Figure 14: Scheme of the bubble dynamics and jet formation during LIFT (Unger et al. 2010)

Many hypotheses have been put forward by researchers to explain the bubble/jet formation, they are(Wang et al. 2009; Xiong et al. 2015):

1. Plasma model;
2. Nucleate boiling model;
3. Phase explosion model;
4. Shock wave model;
5. Thermo-elastic effect model.

However, even though researchers claim that their model is perfectly matched with their experiments, there is no single model that can be proved as the perfect one.

In the plasma model, the optical breakdown is needed to trigger the bubble formation. This process requires a lot of energy, and the energy threshold to trigger it in the water is around 1010 W/cm2 for a nanosecond laser(Kennedy et al. 1995; Vogel et al. 1999), and about 3×1012 W/cm2 for 340 fs laser with 1040 nm wavelength(Vogel et al. 1999). This threshold is too high for most of the laser generators(Lin et al. 2009), which means that the plasma formation cannot be considered as the main reason for the bubble/jet formation.

The boiling model requires the laser pulse duration longer than 100ns, which is also not realistic for most laser types(Lin et al. 2009). Therefore, they consider the phase explosion model as the most promising one to explain the bubble formation in the LAB bioprinting. When the laser energy is absorbed, the bioink is quickly reached and then goes beyond its boiling temperature, and then an equilibrium state of mixed phases is reached.

Xiong et al. (Xiong et al. 2015) applied a nucleation based phase explosion model into their simulation, and the simulation result has a good match with their experimental result, as shown in Figs. 15 and 16.

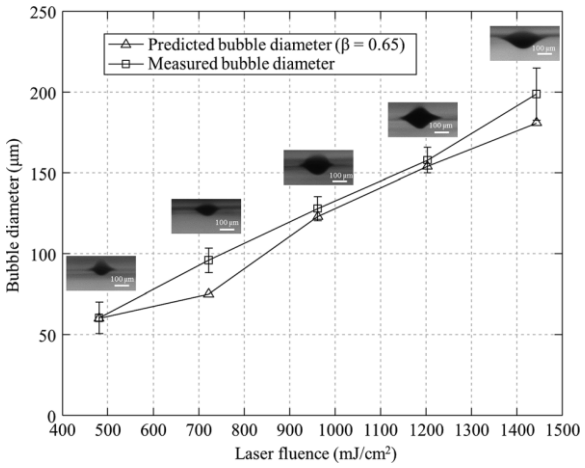

Figure 15: Plot of the transferred droplet volume versus laser pulse energy (Xiong et al. 2015)

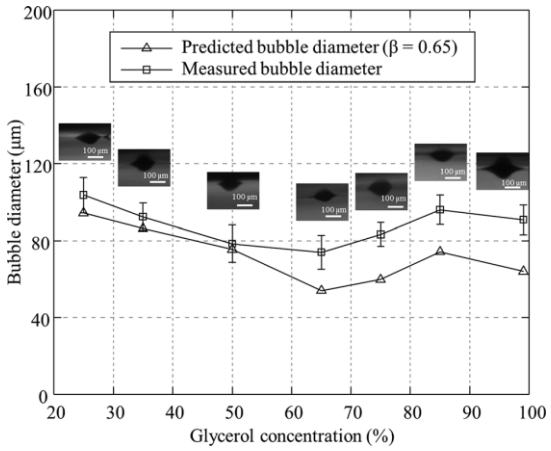

Figure 16: Maximum bubble diameter as a function of glycerol concentration under a 722 mJ/cm^2 laser fluence (Xiong et al. 2015)

To optimize the printing result by controling the bubble/jet formation and improve the cell viability, the physics of bubble/jet formation needs to be studied.

CHAPTER III

EXPERIMENTAL SETUP AND PROTOCOL

3.1 Bioprinter setup

The general bioprinter setup was built according to the LAB theory. The setup is described as follows:

Laser generator

The key equipment of this setup is the laser generator. It is the only power source for the bioink printing. In the experiments, a femtosecond infrared laser generator from Spectra-Physics was used as the source of laser power. It has a laser wavelength at 1040nm, which is in the range of the infrared spectrum. Its laser pulse duration is 300 fs. With 8 watts as its maximum power and produce as high as 200 thousand pulses per second, its maximum pulse power is 40μJ/pulse.

Figure 17: Laser generator

Table 1: Laser specification

	Spirit One 1040-8	Spirit One 1040-8-SHG
Output Characteristics		
Wavelength	1040 ± 5 nm	
Output Power	>8 W	
Pulse Energy	>40 µJ at 200 kHz	
Wavelength (SHG)	NA	520 ± 3 nm
Output Power [2] (SHG)	NA	>4 W at 200 kHz
Pulse Energy [2] (SHG)	NA	>20 µJ at 200 kHz
Repetition Rates[3]	200 kHz or 1 MHz	
Pulse Selection	Integrated pulse picker (AOM) for single shot to 1 MHz operation	
Pulse Width	<400 fs	
Pulse Width Tunability [4,5]	400 fs to 4 ps; tunable by software	
Power Stability	<1% rms over 100 hours (for 1040 nm and 520 nm)	
Pulse-to-Pulse Stability	<2% rms	
Spatial Mode	TEM_{00}, M^2 <1.2	
Beam Diameter (at exit)	2.0 mm (1040 nm); 2.0 mm (520 nm)	
Beam Divergence	<1 mrad (1040 nm); <0.5 mrad (520 nm)	
Pre-Pulse Contrast Ratio	>250:1	
Polarization	Linear	
Cold Start Time	<30 min	
Warm Start Time	<15 min	
Environmental Specifications		
Operating Temperature	18–30°C (64–86°F)	
Humidity	<65%, non-condensing	
Cooling Requirements		
Laser Head	Closed-loop chiller, included with shipment	
Utility Requirements		
Voltage	Laser Head: 24 VDC Chiller: 100-240 V, 50/60 Hz	
Current	<15 A	
Laser Head Physical Characteristics		
Dimensions (L x W x H)	26.2 x 12.2 x 5.2 in (665 x 310 x 133 mm)	29.1 x 12.2 x 5.2 in (740 x 310 x 133 mm)
Weight	88 lb (40 kg)	99 lb (45 kg)
Closed Loop Chiller Physical Characteristics		
Dimensions (L x W x H)	19.0 x 15.8 x 10.5 in (484 x 400 x 267 mm)	
Weight	68 lb (31 kg)	

There is a chiller HECR008-A5 attached to the laser generator to ensure a cool stable temperature of the machine. In this thesis, the chiller was set to 25 C.

Beam expander

After the laser is emitted from the generator, its diameter needs to be expanded. A beam expander was used in the experiments. The beam expander was coaxially installed in front of the laser exit. It will expand the laser diameter to lower the energy density and protect the mirrors and researchers.

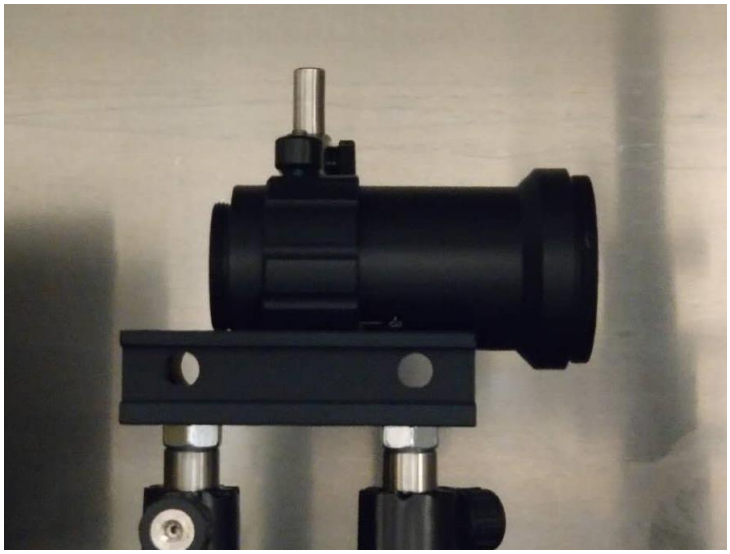

Figure 18: Beam expander

Mirrors and galvanometer

The most important components in the laser path adjusting module are the mirrors. The mirrors are used to arrange the light path and guide it to go into the Galvanometer. And then the galvanometer controls the laser spot in the XY directions.

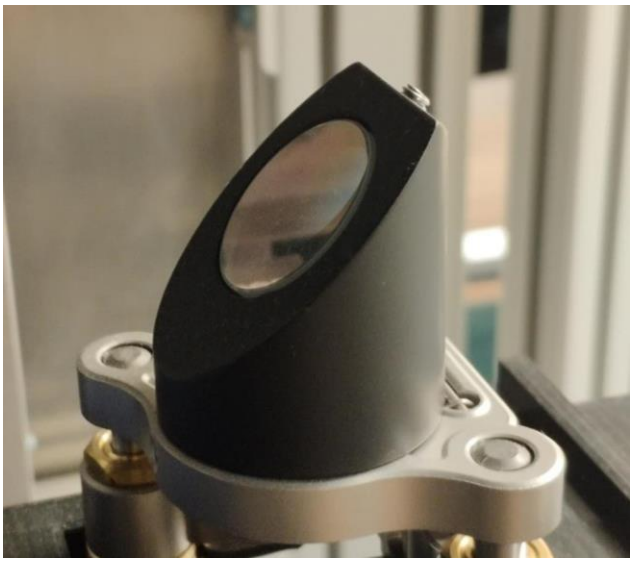

Figure 19: Mirror

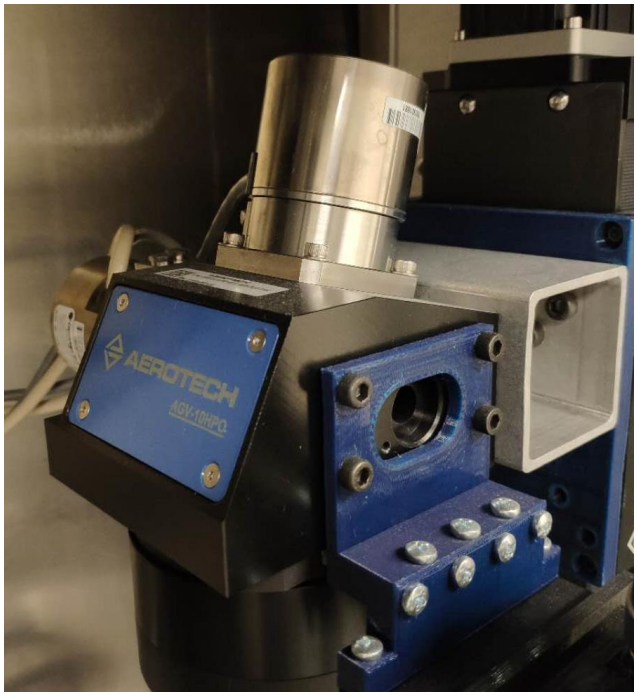

Figure 20: Galvanometer

Focusing lens

During the printing process, the laser should be focused on a small area to pass the energy density threshold of bubble formation. The focusing lens from Thorlabs can achieve an 8μm diameter spot in the 65.1cm focusing distance. It is installed directly underneath the galvanometer.

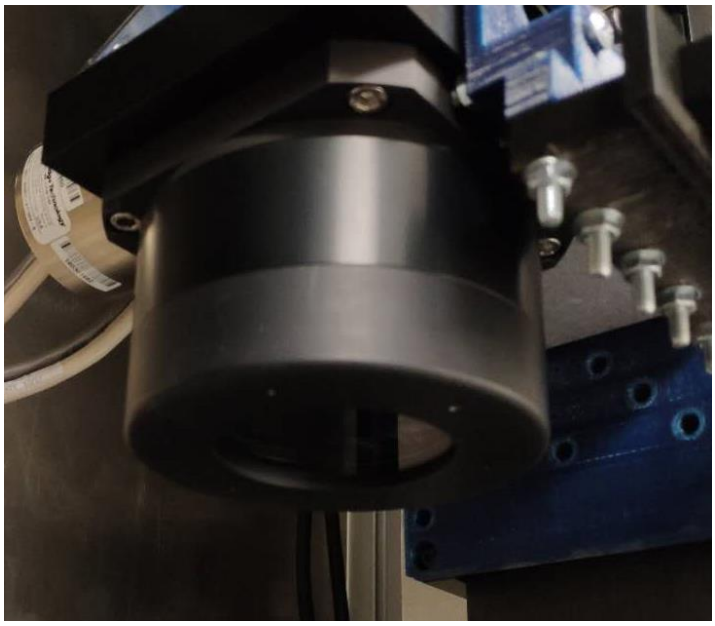

Figure 21: Focusing lens

XYZ stages

The high printing accuracy is one of the most important advantages of LAB. Due to the bucket effect, the printing accuracy is determined by the part in the whole bioprinting system which has the lowest accuracy. In the experiment, the XYZ stages are the components to ensure the droplet deposit in the correct position. In our customized bioprinter, the XY stages are Pro115LM from the Aerotech and the Z stage is Pro115SL from Aerotech. Those stages are capable of high precision movement with an error in the nanometer level.

High-speed camera

It will take only 10 to 100 microseconds for a droplet of bioink to transfer from the ribbon to the substrate. The high-speed camera used in this study was EVO-410L from Phantom.

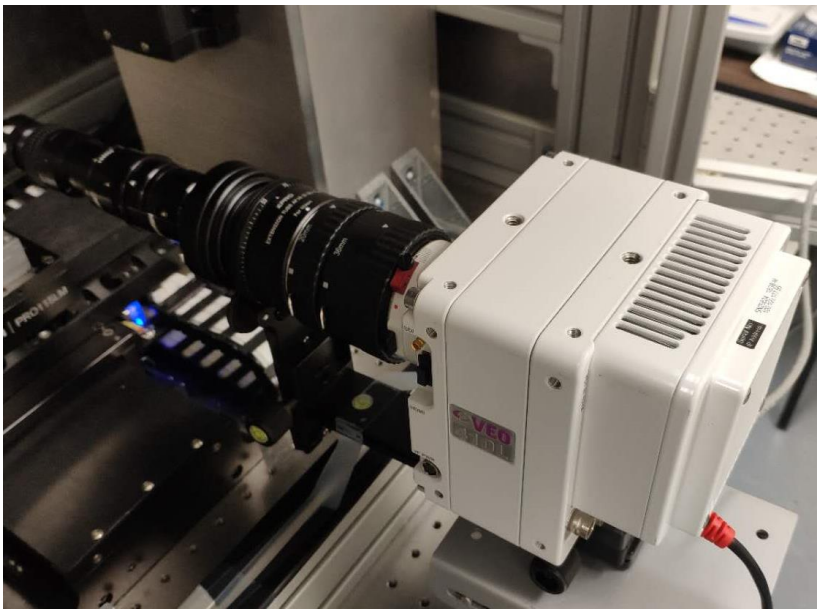

Figure 22: High-speed camera

Light source

When the camera recording at a high frame rate, it requires a great amount of light to feed the sensor. The light source used in this thesis was HL150-A cold light source of halogens from Fisher Scientific.

Figure 23: Light source

The assembled laser assisted bioprinter is as shown in the Figure 24:

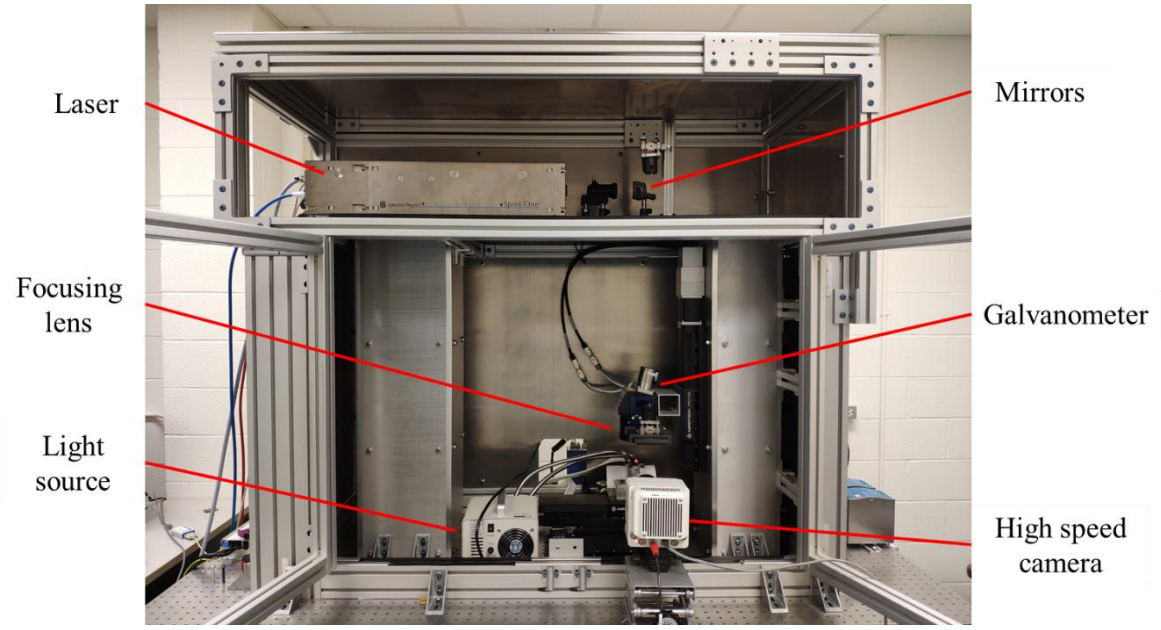

Figure 24: Bioprinter setup

As shown in the Figure, the bioprinter is designed as a two-layer structure to isolate the laser generator and the biomaterial transfer system. The upper layer is composed of a laser

generator, beam expander, and mirrors. In the upper layer, the laser beam is generated and guided to the designed point in the lower layer. Then the laser is focused by the focusing lens and pointing to the printing area by the galvanometer.

The lower layer of the bioprinter equipped with XYZ stages and fixtures. During the printing process, the ribbon and the substrate are held by those fixtures driven by the XY stages. The galvanometer and the focusing lens are attached to the Z stages which can adjust the height of these two parts to make sure the focal point is at the right level on the top surface of the EAL. The light source and the high-speed camera comprise the observation system which can be used to observe the formation of the bioink jet. The fiber light and the CCD are placed facing each other to make sure the sensor can obtain the maximum background light and record the clear profile of the droplet/jet.

3.2 Printing parameters

From the discussions in chapter 2, apparently, the performance of the LAB is highly dependent on the values of printing parameters, which determines many key features of the LAB such as the shape of the jet, deposit volume, resolution, and cell viability. Among all parameters, those related to the laser and energy absorbing performance have more importance than others because those parameters are directly related to the bioink transfer process. This thesis selected two major printing parameters regarding laser energy to study, they are:

1. Laser pulse energy
2. The thickness of the energy absorbing layer

The laser pulse energy is how many joules of energy contained in a single laser pulse. This energy will be absorbed by the EAL, consequently, melt or vaporize the EAL and generate a vapor bubble which is a key step to form a jet and deposit bioink on the substrate. The laser used in this thesis has the highest laser pulse energy of 40μJ per pulse and can be adjusted from 1-100% power level. According to the manufacturer, the laser will operate stably above its 10% maximum power, which means it has a stable laser pulse energy range from 4μJ to 40μJ. This thesis set 4 different energy levels with a 10μJ gap in between to analyze the influence of the laser pulse energy, they are 10μJ, 20μJ, 30μJ, and 40μJ.

It is noteworthy that the laser pulse energy cannot be 100% utilized by the printing process, there is another factor that plays an important role in this, which is energy absorption. The energy absorbing layer (EAL) is a specially designed layer coated on the ribbon to provide efficient laser energy absorbing performance. Its laser absorbing performance depends on its material and thickness. The most common material used to build an EAL is titanium and gold, both provide good protection for the biomaterial and has a better absorption rate of laser than bioink. The thickness of the metal EAL is usually around 10nm.

In this study, the graphene was used as the material of the EAL to provide enough laser absorption and biocompatibility. The thickness of the graphene EAL was studied as another essential parameter of LAB printing. Different from the metal or metal oxide EALs, the graphene is not opaque and cannot reflect the laser. Thus, its penetration depth is longer than metal or metal oxide. The wildly applied rule for the EAL is that for protecting the biomaterial, is its thickness must larger than the laser penetration depth, however, the difference between graphene and metal makes it hard to fulfill that request. From another point of view, the thickness of the EAL may not be so important. One of the LAB types is MAPLE-DW, which is a bioprinting

technology without EAL, has cell viability not so worse than the AFA-LIFT. In this case, this thesis test 5 different thickness of graphene EALs, they are 0.22μm, 0.44μm, 0.66μm, 0.88μm, and 1.10μm. The graphene EAL is made by coating the water-based graphene dispersion on the ribbon and dry it out. Those thickness are corresponding to the coated graphene dispersion thickness of 0, 25μm, 50μm, 75μm, 100μm, and 125μm.

For example, if 0.44μm graphene EAL is needed, the thickness of the graphene dispersion can be calculated as follows:

$$0.44um = 0.44 \times 10^{-6}m$$

The true density of the graphene is$2.27g/cm^3$ which equals to$2.27 \times 10^6 g/m^3$.

On the coated area, the graphene per area is:

$$0.44 \times 10^{-6}m \times 2.27 \times \frac{10^6 g}{m^3} = 1.00g/m^2$$

The density of the 1wt% graphene water-based graphene dispersion approximately equals to $1 \times 10^6 g/m^3$.

The graphene in the dispersion is:

$$1 \times \frac{10^6 g}{m^3} \times 1\% = 1 \times 10^4 g/m^3$$

The thickness of the dispersion applied should be:

$$\frac{1.00g}{m^2} \div 1 \times \frac{10^4 g}{m^3} = 1.00 \times 10^{-4}m = 100um$$

3.3 Experimental protocol for orthogonal experiments

There were eight sets of experiments designed in the orthogonal experiments. All those experiments are orthogonalized to study the impact of different parameters in LAB printing.

The two main parameters tested and discussed in this thesis was the laser pulse power and the layer thickness of the graphene EAL. The experiment plan is listed in the form below.

Table 2: The experiments set table

EAL thickness/Laser pulse energy	10 μJ	20 μJ	30 μJ	40 μJ
0.22 um	Group 1	Group 2	Group 3	Group 4
0.44 um	Group 5	Group 6	Group 7	Group 8
0.66 um	Group 9	Group 10	Group 11	Group 12
0.88 um	Group 13	Group 14	Group 15	Group 16
1.10 um	Group 17	Group 18	Group 19	Group 20

3.4 Preparation of the experiments

3.4.1 Preparation of the graphene EAL

The transparent ribbon used in those experiments was glass slides from the Fisher brand. The glass slide is 25 mm in depth, 75 mm in width, and 1mm in thickness and transparent to 1040 nm infrared laser.

The graphene EAL was coated by spreading the water-based graphene dispersion on the ribbon evenly. The graphene dispersion was bought from the US Nano company. Before coating, the glass slide was cleaned sequence by distilled water, isopropyl alcohol, and then by lens

paper. The tape was used to help to coat the graphene dispersion on the ribbon by accurate thickness.

The photo of the EALs are as follows:

Figure 25: Ribbon with 0.22µm graphene energy absorbing layer

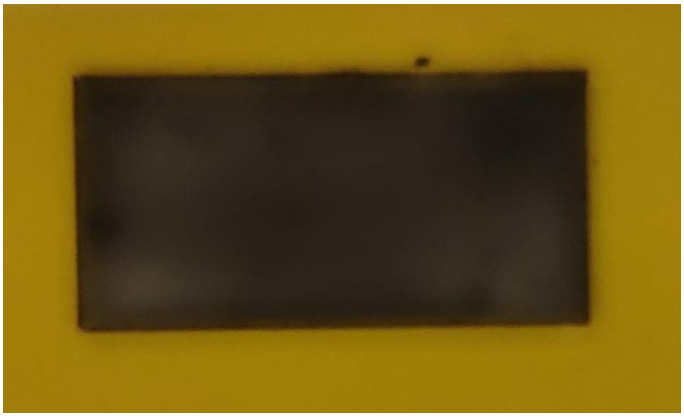

Figure 26: Ribbon with 0.44µm graphene energy absorbing layer

Figure 27: Ribbon with 0.66µm graphene energy absorbing layer

Figure 28: Ribbon with 0.88µm graphene energy absorbing layer

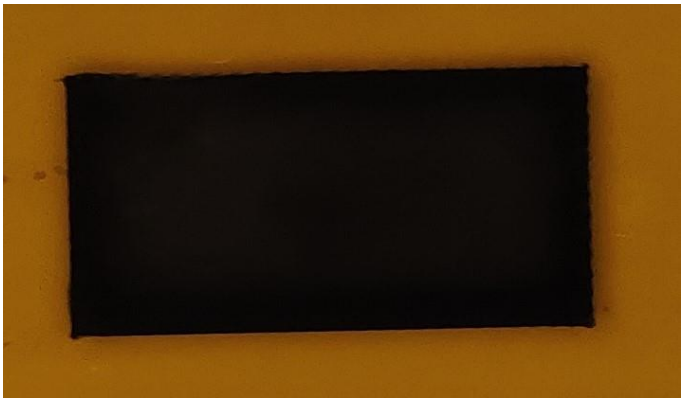

Figure 29: Ribbon with 1.12µm graphene energy absorbing layer

Once the graphene dispersion was applied on the slide, the ribbon was placed on a heater from Thermo Scientific and dried at 50 Celsius degree.

3.4.2 Preparation of the substrate

The same glass slide was also used as the receiving substrate because its high transparency is good for the microscope observation after printing. Tape stacks were used to construct an equal height curb at both ends of the slide to ensure the bioink travel distance between the ribbon and the substrate.

3.4.3 Preparation of the bioink

The glycerol-water solution was used as the bioink in the bioprinting experiment. To achieve a suitable viscosity and prevent the rapid evaporation, the concentration of the glycerol was set to 67%. The volume-based blade coating method was used to coat the glycerol-water solution on the ribbon evenly.

CHAPTER IV

RESULTS AND DISCUSSION

4.1 Protocol of experiments

The ribbon and the substrate were prepared before the start. The whole protocol of the experiment in this study was:

1. The laser security lock is turned off and the laser generator is set to power on mode. The physical shutter is open. The chiller is continuously on at 25C to stabilize the temperature of the laser system.
2. Open the laser control software and click “connect”. Set the “Laser Output Enable” and “Laser Output Modulation” to external, which enables the A3200 Motion Composer software to take over the laser generator.
3. Set the “Repetition Rate” at 200K and the “Pulse Picker Divider” at 10000, which indicates the laser repeating rate of the laser is 20 pulse per second.
4. Open the A3200 Motion Composer and enable X, Y, Z, GX, and GY. After checking the stages to make sure there is no physical block of the movement, home X, Y, Z, GX, and GY.
5. Prepare the ribbon and the substrate. Install them on the fixture and locate the printing area.

6. Adjust the position and the height of the camera letting the field of view cover the jetting area (laser focal point) and then adjust the camera lens to the designed magnification.Turn the laser to stand by mode. Open the inner shutter.
7. Turn the laser on and operate a warmup set.
8. Run the program, print the bioink.
9. Adjust the parameters for the next set.

4.2 Experiments results

4.2.1 Observation equipment

Based on the experiment method introduced in the previous chapter, in this chapter, the customized LAB printer was used to test the printing result. The printed samples were observed and measured under the microscope. By comparing samples printed by different laser pulse energy and EAL thickness, the performance of the graphene EAL is discussed.

The high-speed camera Evo 410L was used to observe and record the bubble/jet formation process for future analysis. The resolution was set to 256x256 pixels and the footage was filmed at 57000 frames per second, which means frames will take every 17.5μs.

4.2.2 Bubble/jet formation

The groups with a 0.22μm thickness graphene EAL set were chosen to be recorded. The laser pulse energies were 10μJ, 20μJ, 30μJ, and 40μJ respectively. 12 frames from each video are selected to present the LAB bioprinting process. They are the first few frames at the bubble/jet formation and keyframes during the bioink transfer process. Those frames are listed as follows:

Group1 with 10μJ laser power

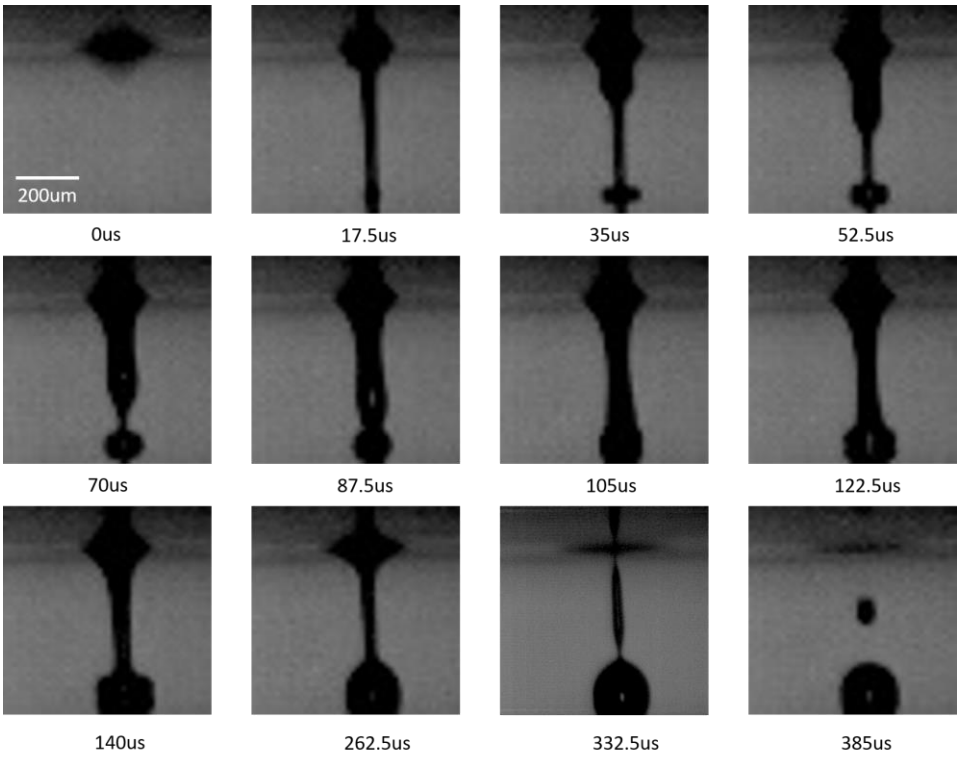

Figure 30: The bubble/jet formation with 0.22µm graphene EAL and 10µJ laser pulse power

With the condition of 0.22µm graphene EAL, the 10µJ laser pulse power generated a bubble at around 200µm diameter in the bioink layer. The jet was fully developed in 17.5µs with a diameter of about 40µm and a droplet at 100µm was created on the substrate. After the jet reached the lower substrate, there was more bioink transferred through the jet in 300µs and the droplet on the substrate gets much larger to 170µm.

Group2 with 20μJ laser power

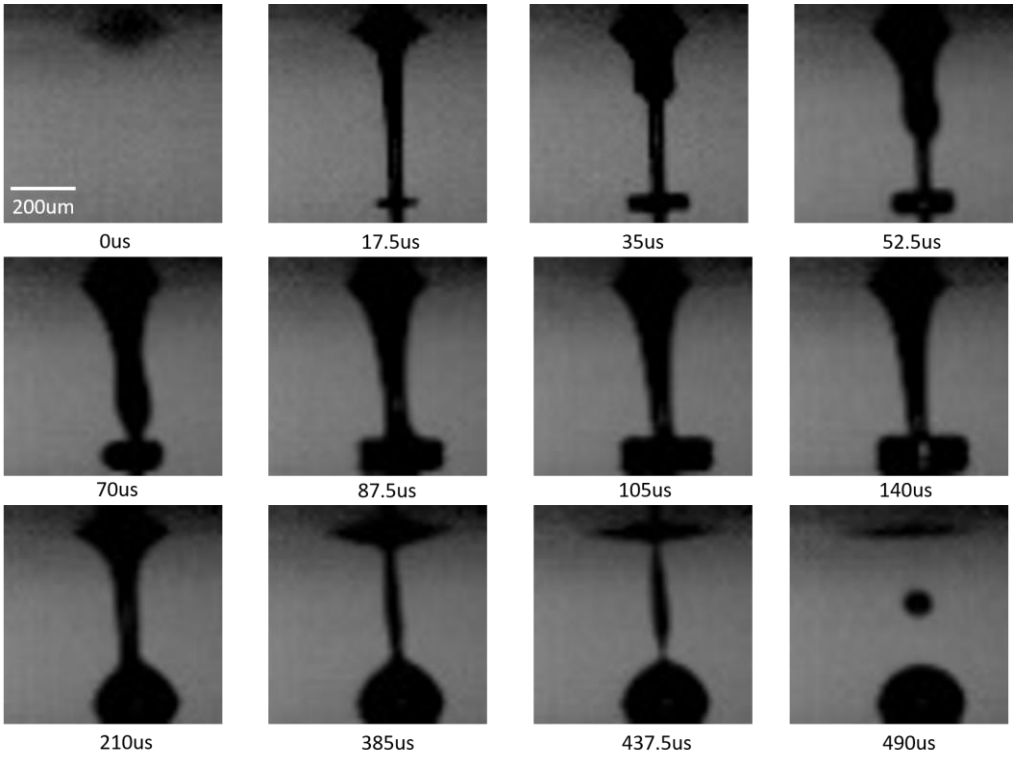

Figure 31: The bubble/jet formation with 0.22µm graphene EAL and 20µJ laser pulse power

Similar to the last set, the bubble was about 200µm in diameter and the jet reached the substrate in 17.5µs. However, the jet was stronger than in the 10µJ case, its diameter grows to 50µm instead of 40µm and more bioink was transferred via jet afterward. The final droplet on the substrate was around 220µm in diameter.

Group3 with 30μJ laser power

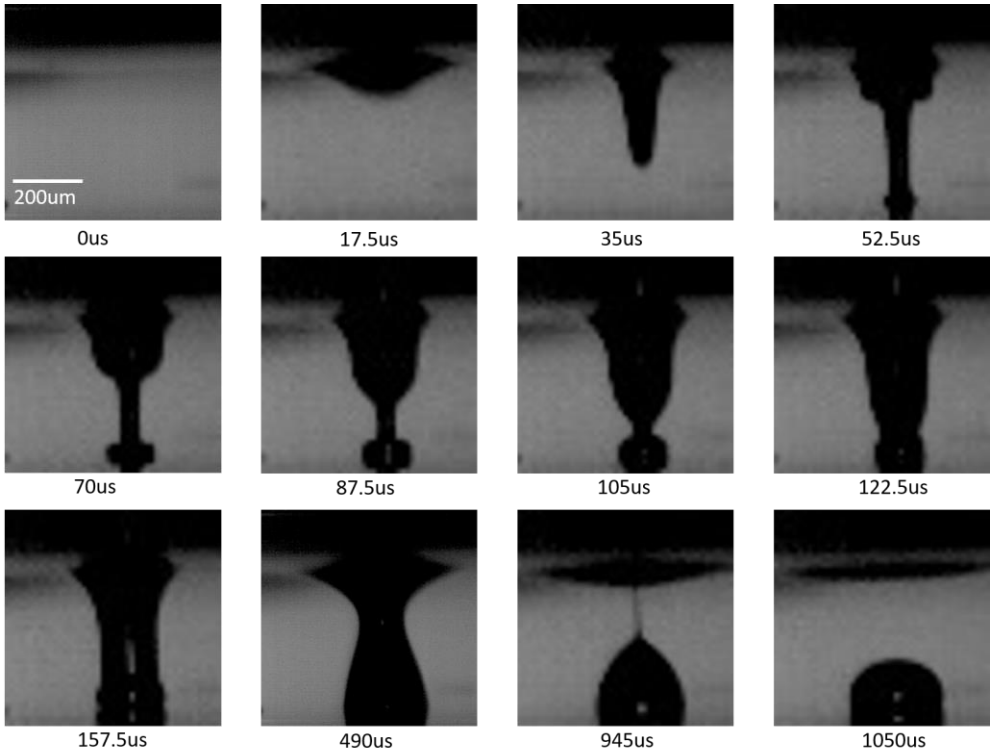

Figure 32: The bubble/jet formation with 0.22µm graphene EAL and 30µJ laser pulse power

In the 30µJ laser pulse power set, the bubble grew to about 250µm in diameter. The jet in this case developed in 35µs, which is much slower than in previous cases. There was more bioink transferred after the jet was fully developed. A 260µm diameter droplet left on the substrate after printing.

Group4 with 40μJ laser power

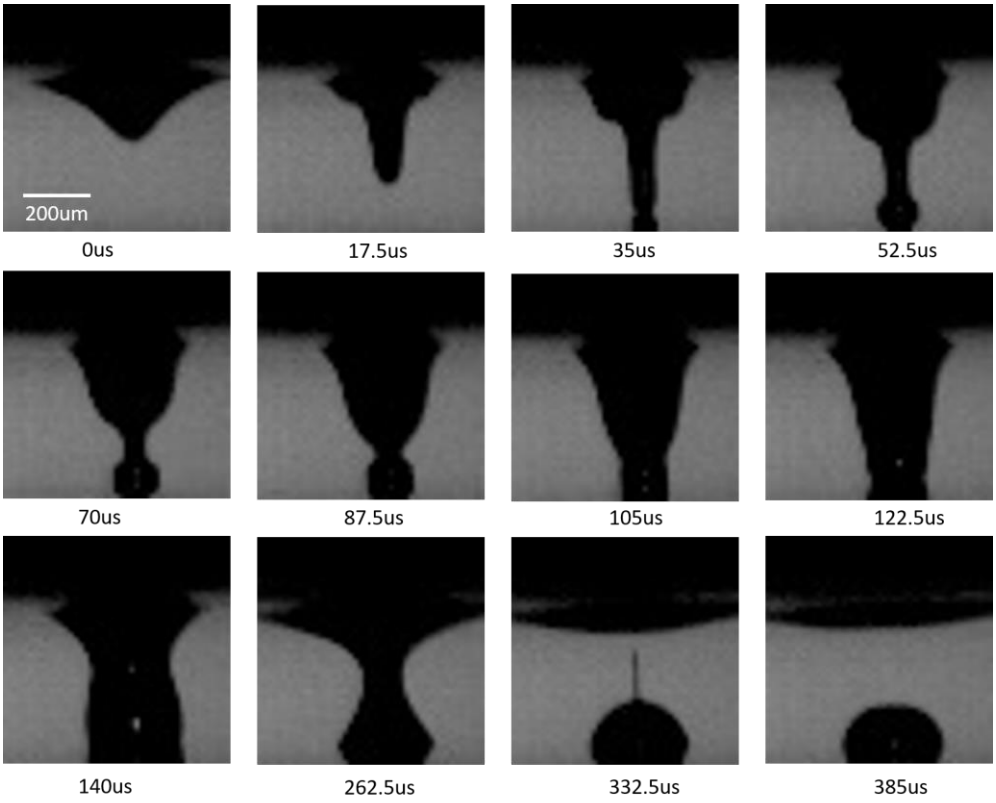

Figure 33: The bubble/jet formation with 0.22µm graphene EAL and 40µJ laser pulse power

The 40µJ laser pulse power is the maximum power the laser generator can obtain. What can be concluded from the frames is that the jet diameter was not significantly changed, but the amount of the bioink that went through the jet and deposit on the substrate was increased. The post-printing droplet has a diameter of about 300µm, which is the largest in all four sets.

4.2.3 The energy absorbing layer

The energy absorbing layer (EAL) plays an important role in the LAB as a laser absorbing part. In most cases, the EAL will be broken or vaporized. Observing the EAL after the printing can give researchers information about the laser energy, laser affected zone, and further provide the evidence to analysis the bioink contamination and cell viability.

Having a good contrast of the vaporized area, the 0.88μm graphene EAL was selected to be taken photos on. The ribbon was transferred to the microscope after the bioprinting for the observation of the EAL. Those photos are list as follows:

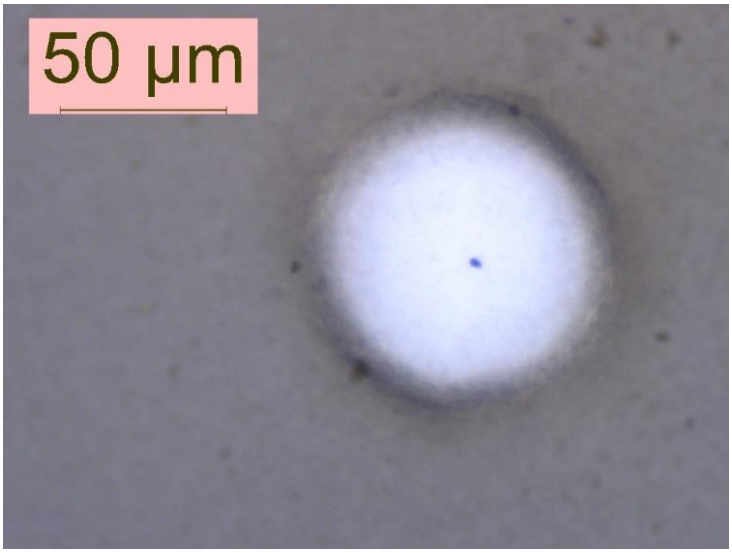

Figure 34: 0.88μm graphene EAL after radiated by 10μJ laser pulse

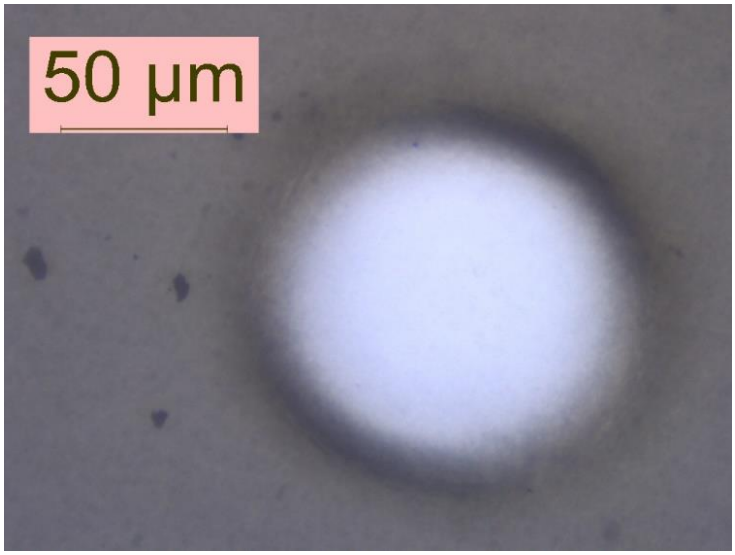

Figure 35: 0.88µm graphene EAL after radiated by 20µJ laser pulse

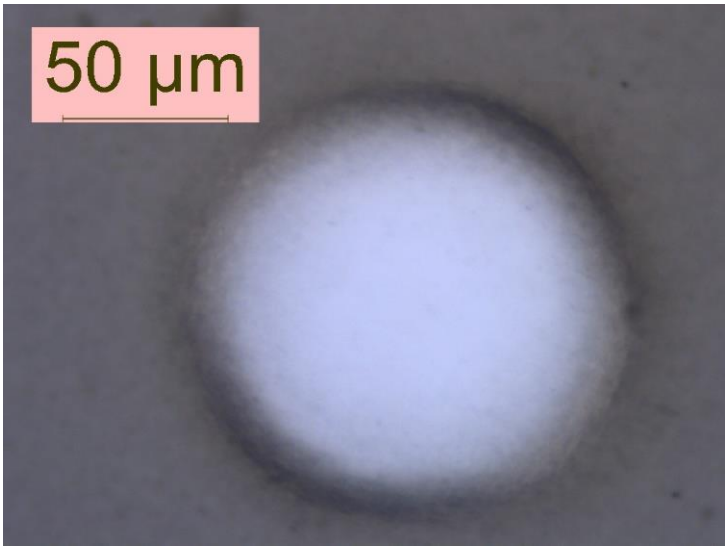

Figure 36: 0.88µm graphene EAL after radiated by 30µJ laser pulse

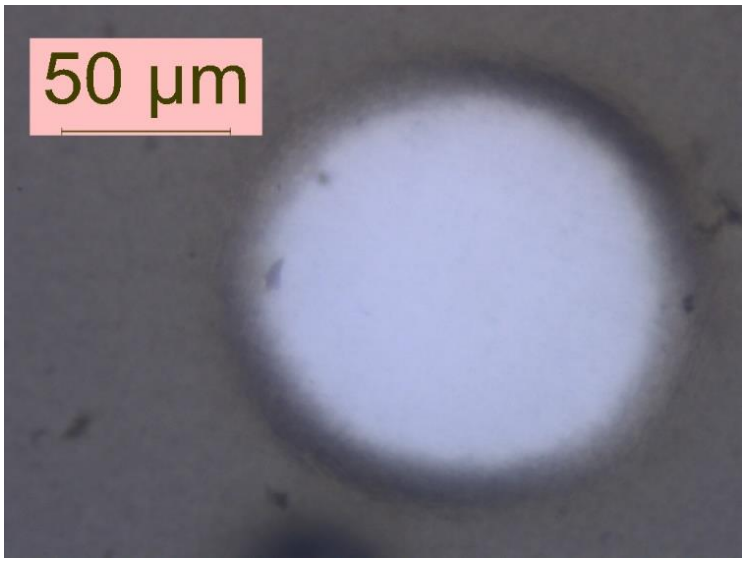

Figure 37: 0.88µm graphene EAL after radiated by 40µJ laser pulse

Measured under the microscope (LEICA MC 170 HD), the laser pulse with 10µJ, 20µJ, 30µJ, and 40µJ creates broken holes on the EAL with diameters 80µm, 100µm, 113µm, and 120µm respectively.

Table 3: The affected zone diameters of different laser pulse energy

Laser(µJ)	10	20	30	40
Affected zone(µm)	80	100	113	120

The laser affected zone is getting larger when the laser pulse energy increases. This is because the laser obeys the Gaussian distribution and the energy level of the outer ring evaluated when the laser energy increased.

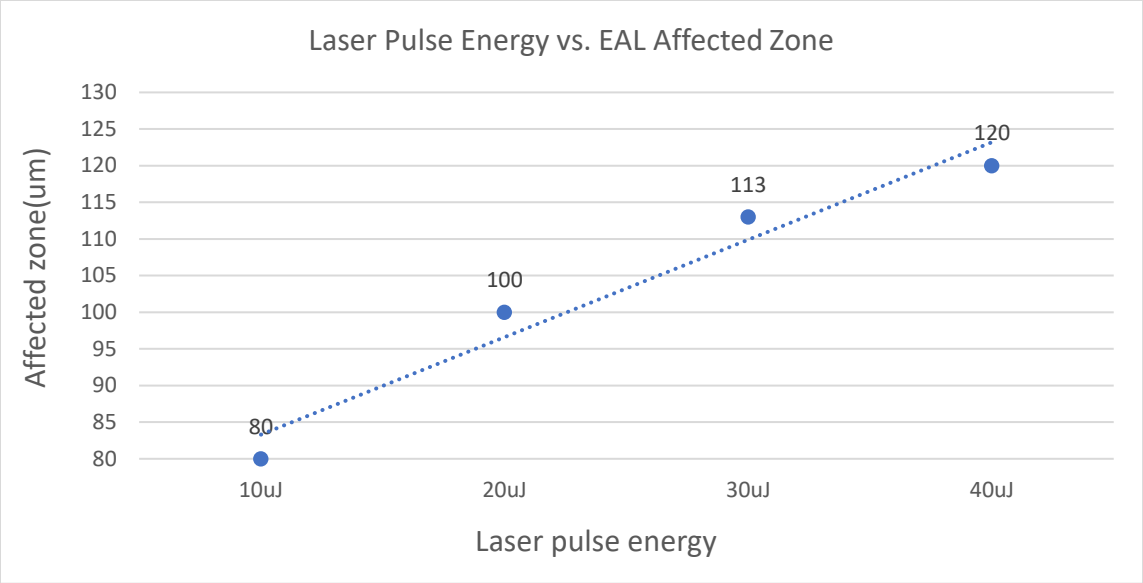

Figure 38: Laser Pulse Energy vs. EAL Affected Zone

In the laser pulse energy range of 10μJ to 40μJ, the affected zone size can be considered as liner to the laser pulse energy with the scope 1.5μm/μJ, which means with every 1μJ increase in the laser pulse energy, the EAL affected zone size will increase 1.5μm.

4.2.4 Bioprinting result

For all experimental sets, the substrate was immediately observed using the microscope. All photos of droplets were taken under 5x, 20x objective lenses. Some small drops were observed further by 50x objective lenses.

The photos of the droplets are listed as follows:

Group1: 0.22 graphene EAL and 10µJ laser pulse energy

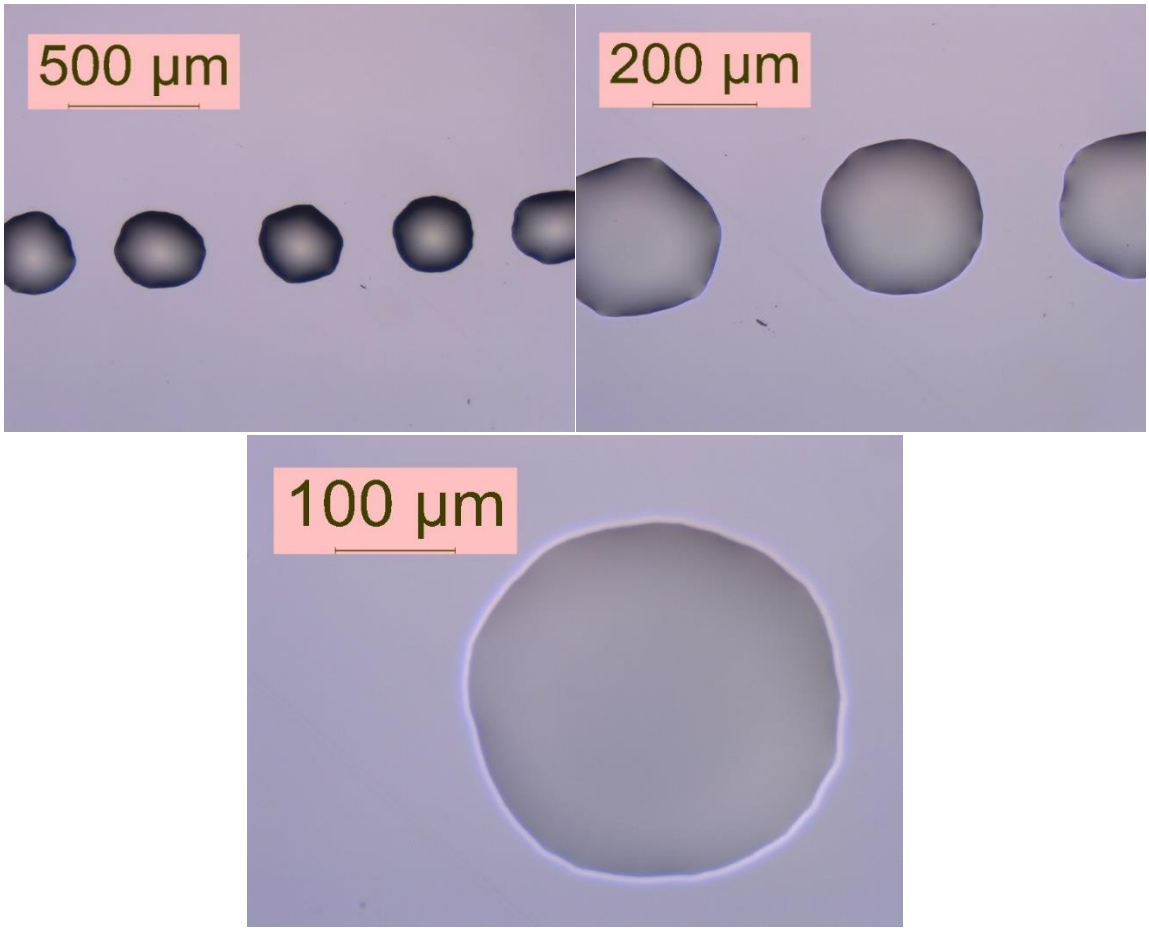

Figure 39: Bioink transferred on the substrate with 0.22 graphene EAL and 10µJ laser pulse energy

With 0.22µm graphene EAL and 10µJ laser pulse energy, the droplets deposited on the substrate were evenly distributed with 500µm gaps in between. All droplets were in regular round shape. The diameter of the droplet was about 300µm.

Group2: 0.22 graphene EAL and 20µJ laser pulse energy

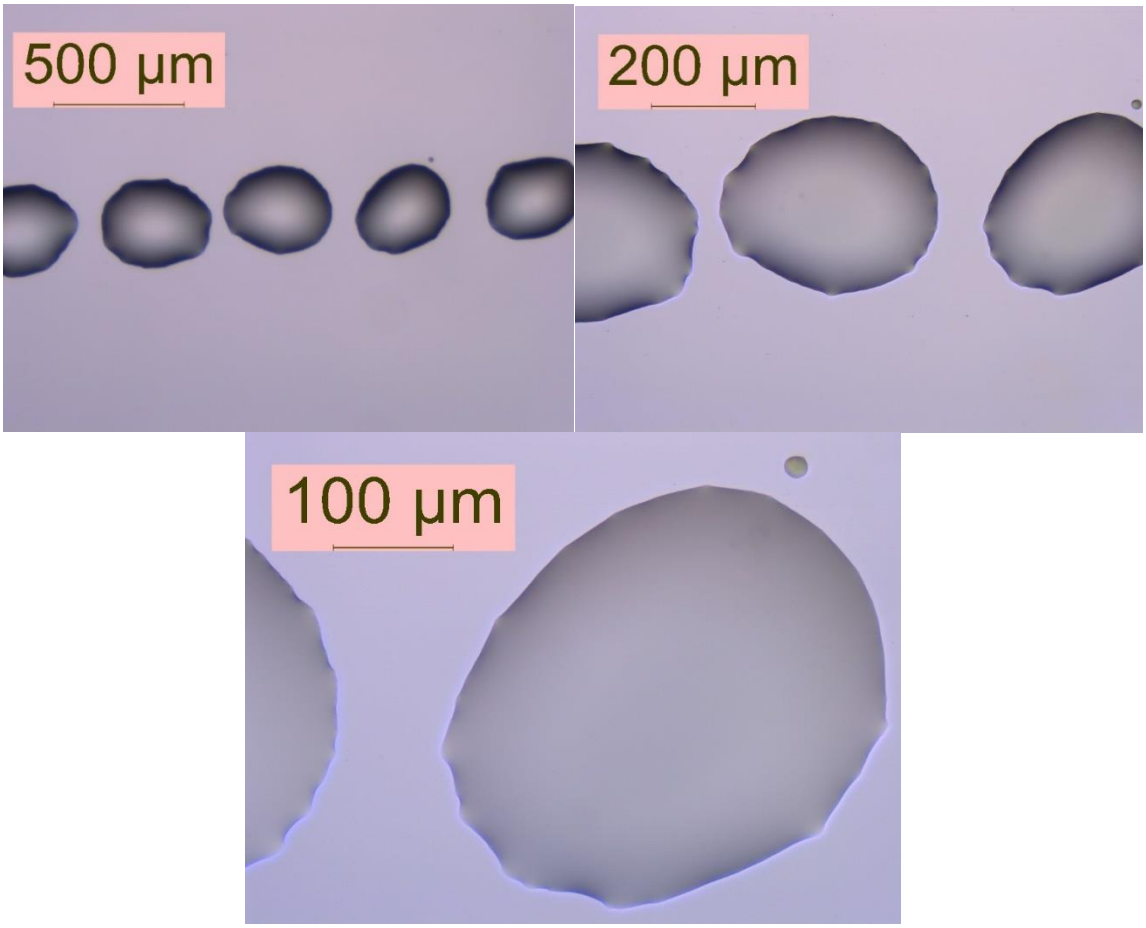

Figure 40: Bioink transferred on the substrate with 0.22 graphene EAL and 20µJ laser pulse energy

With 0.22µm graphene EAL and 20µJ laser pulse energy, the droplets deposited on the substrate were evenly distributed with 500µm gaps in between. All droplets were in ellipse shape. The diameter of the droplet was about 340µm.

Group3: 0.22 graphene EAL and 30µJ laser pulse energy

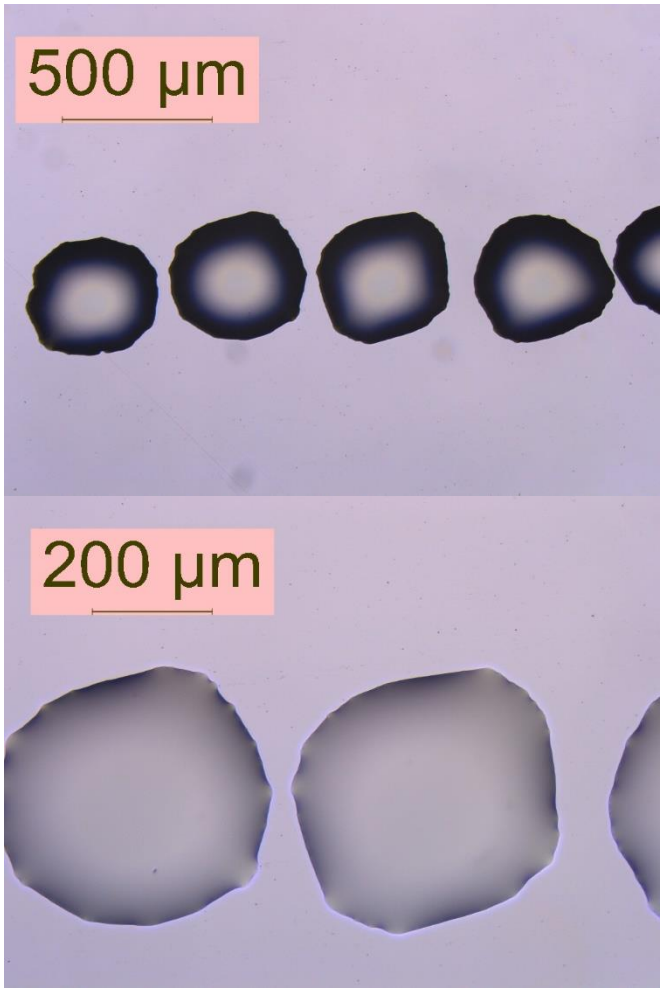

Figure 41: Bioink transferred on the substrate with 0.22 graphene EAL and 30µJ laser pulse energy

With 0.22µm graphene EAL and 30µJ laser pulse energy, the droplets deposited on the substrate were evenly distributed with 500µm gaps in between. All droplets were in irregular round shape. The diameter of the droplet was about 400µm.

Group4: 0.22 graphene EAL and 40µJ laser pulse energy

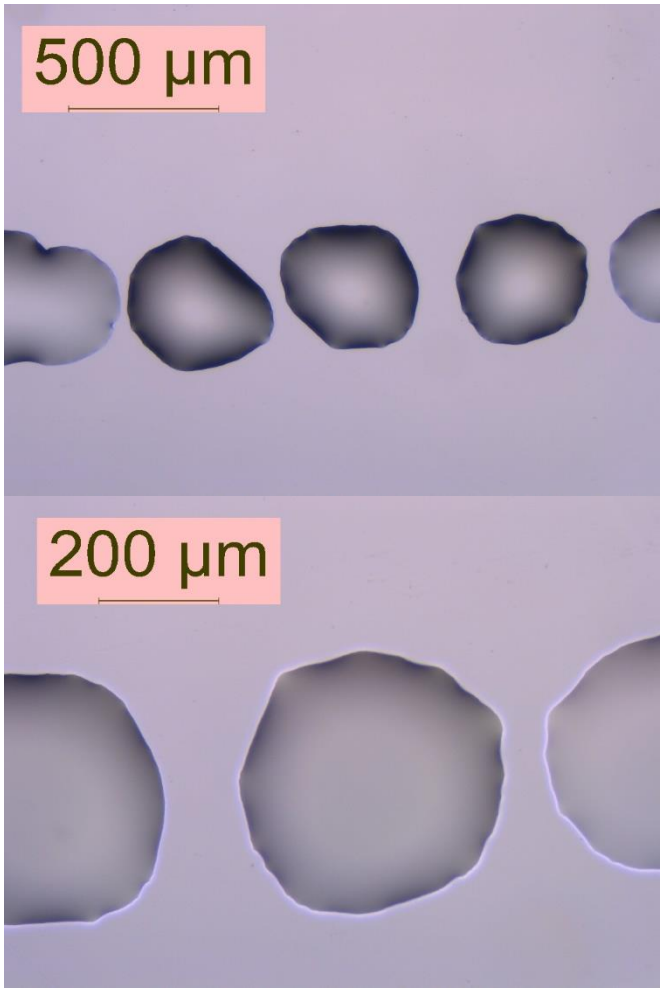

Figure 42: Bioink transferred on the substrate with 0.22 graphene EAL and 40µJ laser pulse energy

With 0.22µm graphene EAL and 40µJ laser pulse energy, the droplets deposited on the substrate were evenly distributed with 500µm gaps in between. All droplets were in irregular round shape. The diameter of the droplet was about 440µm.

Group5: 0.44 graphene EAL and 10µJ laser pulse energy

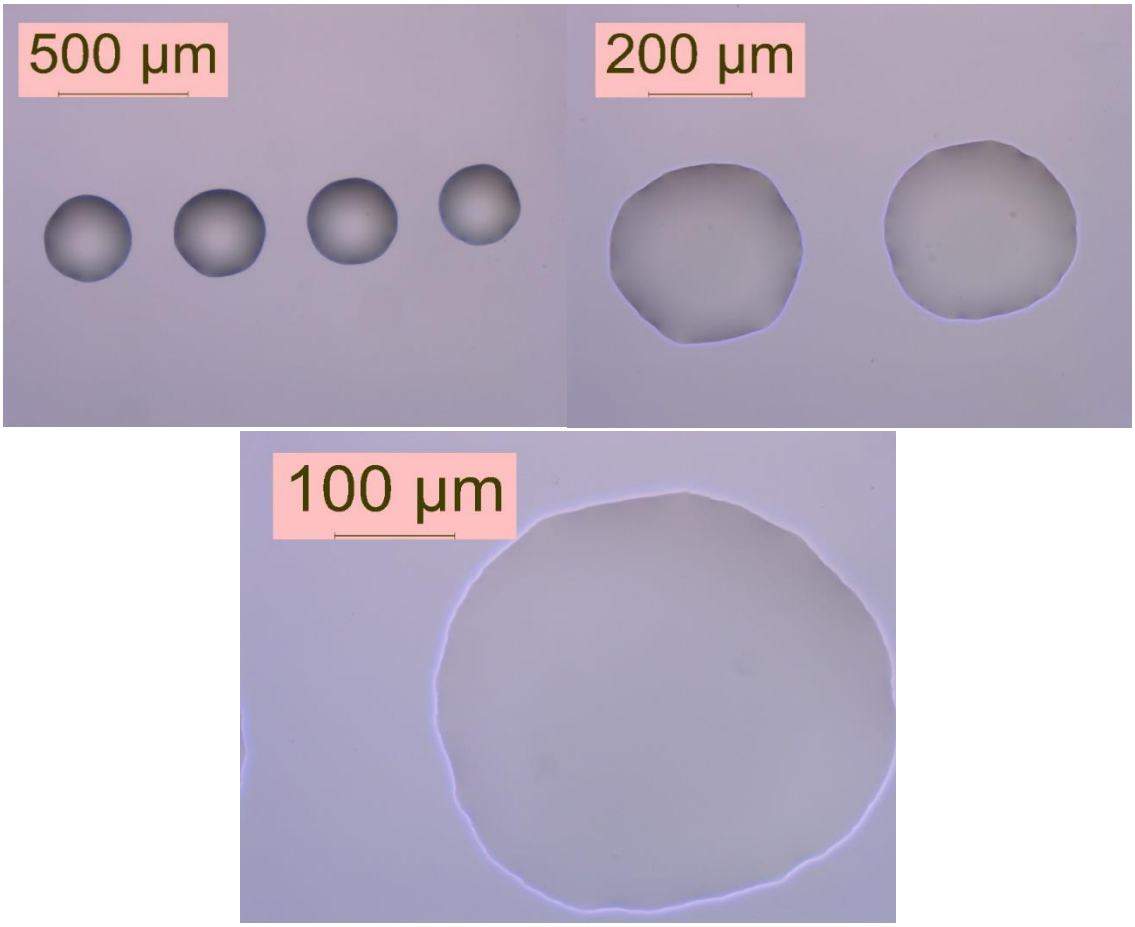

Figure 43: Bioink transferred on the substrate with 0.44 graphene EAL and 10µJ laser pulse energy

With 0.44µm graphene EAL and 10µJ laser pulse energy, the droplets deposited on the substrate were evenly distributed with 500µm gaps in between. All droplets were in regular round shape. The diameter of the droplet was about 340µm.

Group6: 0.44 graphene EAL and 20µJ laser pulse energy

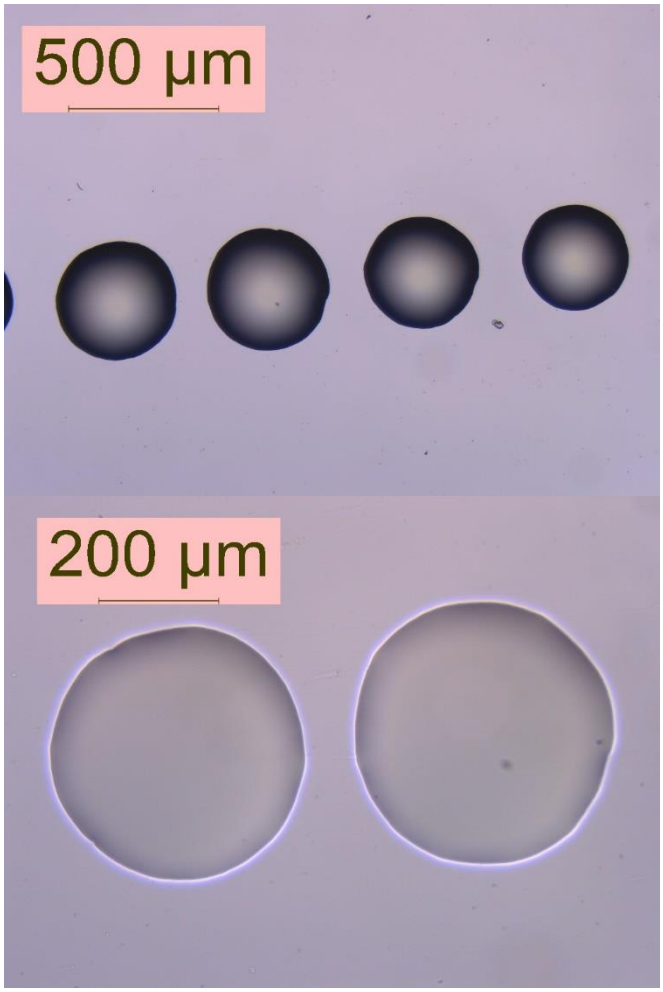

Figure 44: Bioink transferred on the substrate with 0.44 graphene EAL and 20µJ laser pulse energy

With 0.44µm graphene EAL and 20µJ laser pulse energy, the droplets deposited on the substrate were evenly distributed with 500µm gaps in between. All droplets were in regular round shape. The diameter of the droplet was about 400µm.

Group7: 0.44 graphene EAL and 30µJ laser pulse energy

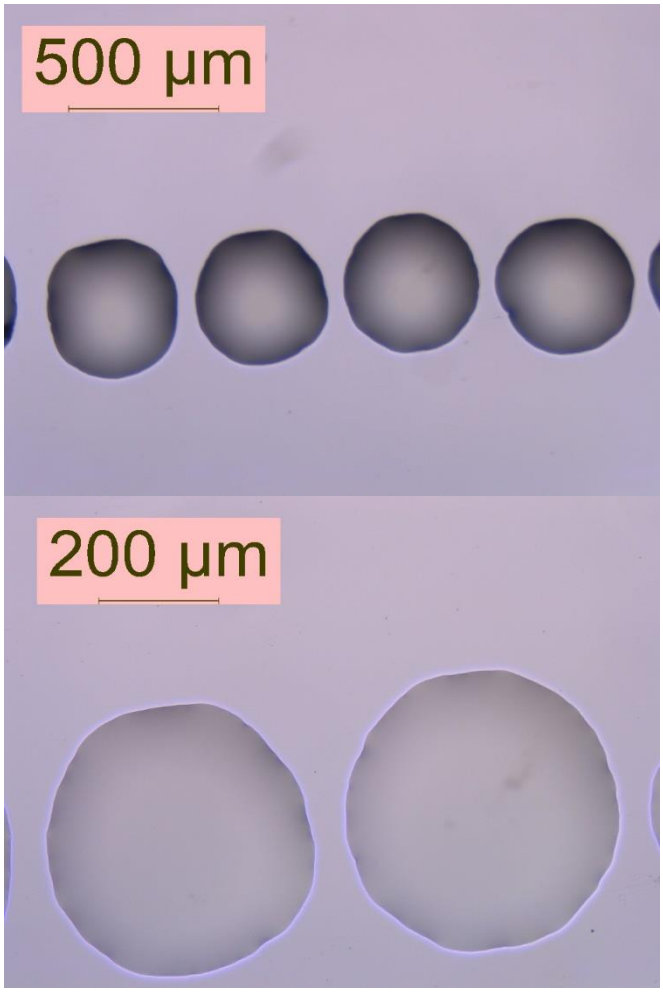

Figure 45: Bioink transferred on the substrate with 0.44 graphene EAL and 30µJ laser pulse energy

With 0.44µm graphene EAL and 30µJ laser pulse energy, the droplet deposit on the substrate is evenly distributed with a 500µm gap in between. All droplets were in regular round shape. The diameter of the droplet was about 450µm.

Group8: 0.44 graphene EAL and 40µJ laser pulse energy

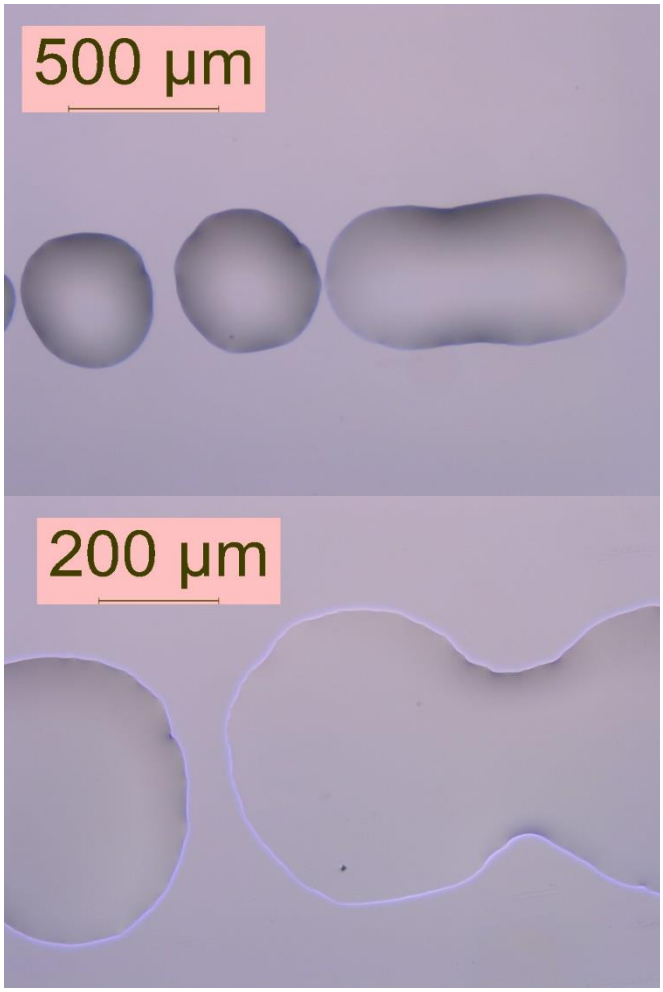

Figure 46: Bioink transferred on the substrate with 0.44 graphene EAL and 40µJ laser pulse energy

With 0.44µm graphene EAL and 30µJ laser pulse energy, the droplets deposited on the substrate were evenly distributed with 500µm gaps in between. Some droplets were connected. The diameter of the droplet was about 450µm.

Group9: 0.66 graphene EAL and 10µJ laser pulse energy

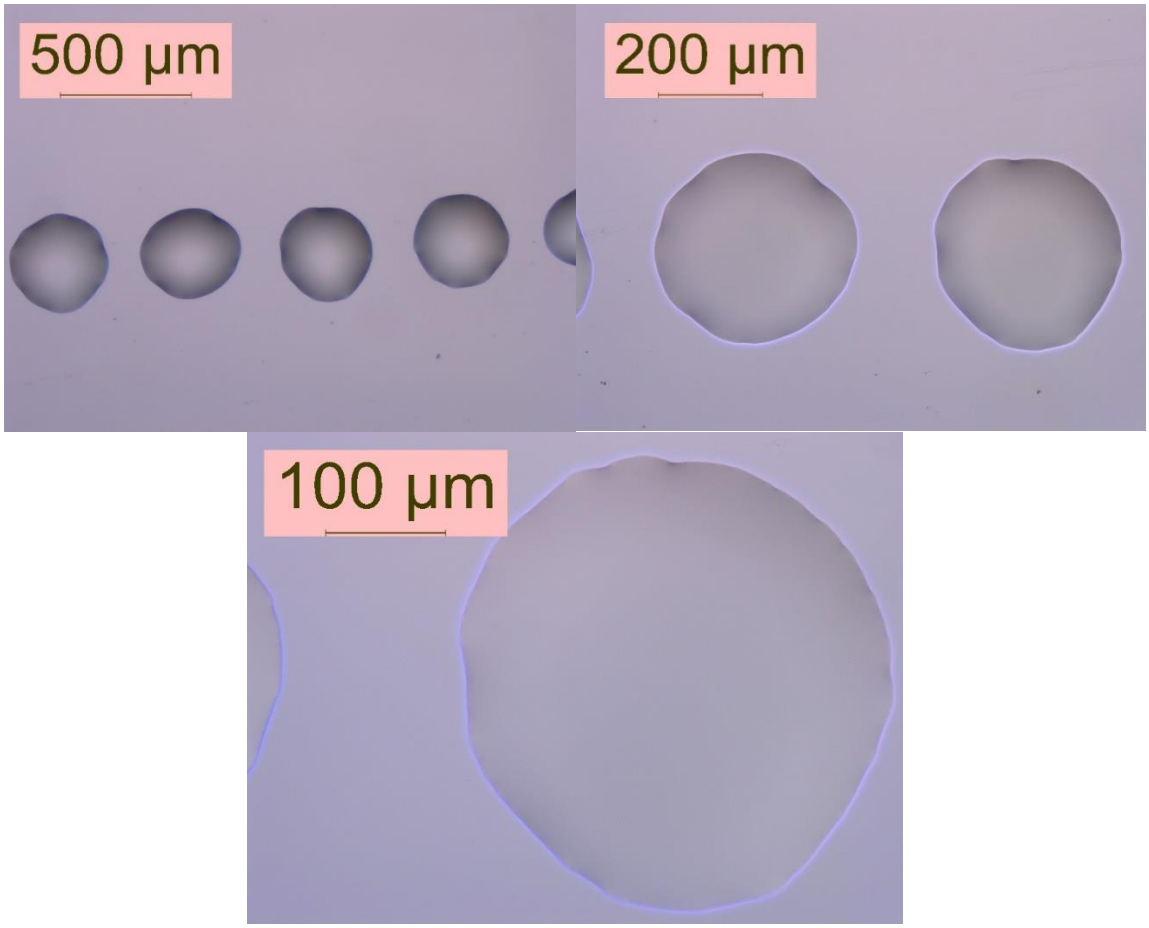

Figure 47: Bioink transferred on the substrate with 0.66 graphene EAL and 10µJ laser pulse energy

With 0.66µm graphene EAL and 10µJ laser pulse energy, the droplets deposited on the substrate were evenly distributed with 500µm gaps in between. All droplets were in irregular round shape. The diameter of the droplet was about 350µm.

Group10: 0.66 graphene EAL and 20μJ laser pulse energy

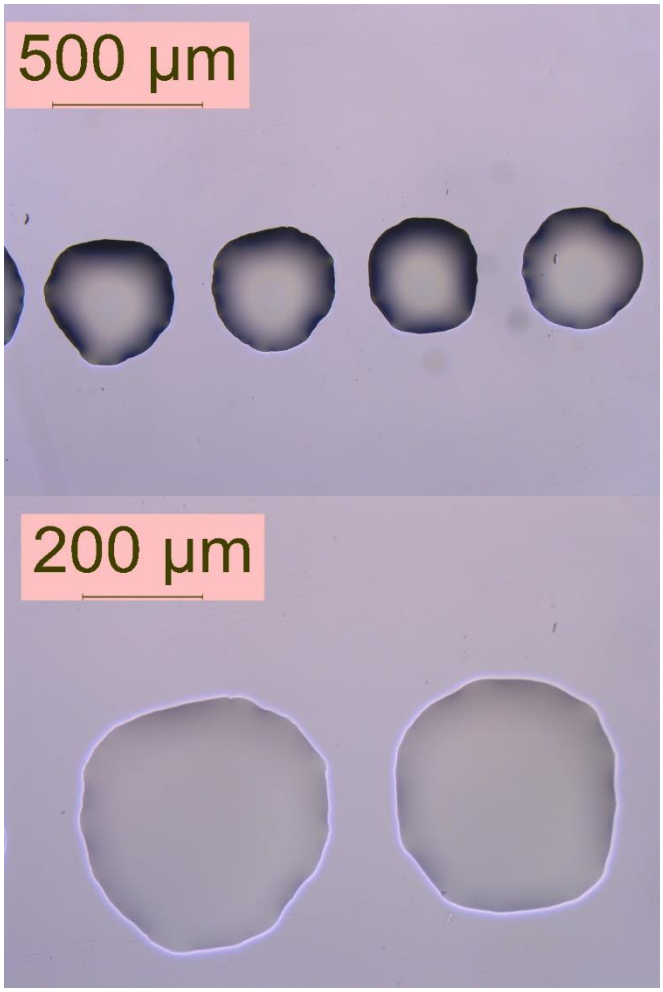

Figure 48: Bioink transferred on the substrate with 0.66 graphene EAL and 20μJ laser pulse energy

With 0.66μm graphene EAL and 20μJ laser pulse energy, the droplets deposited on the substrate were evenly distributed with 500μm gaps in between. All droplets were in irregular round shape. The diameter of the droplet was about 390μm.

Group11: 0.66 graphene EAL and 30μJ laser pulse energy

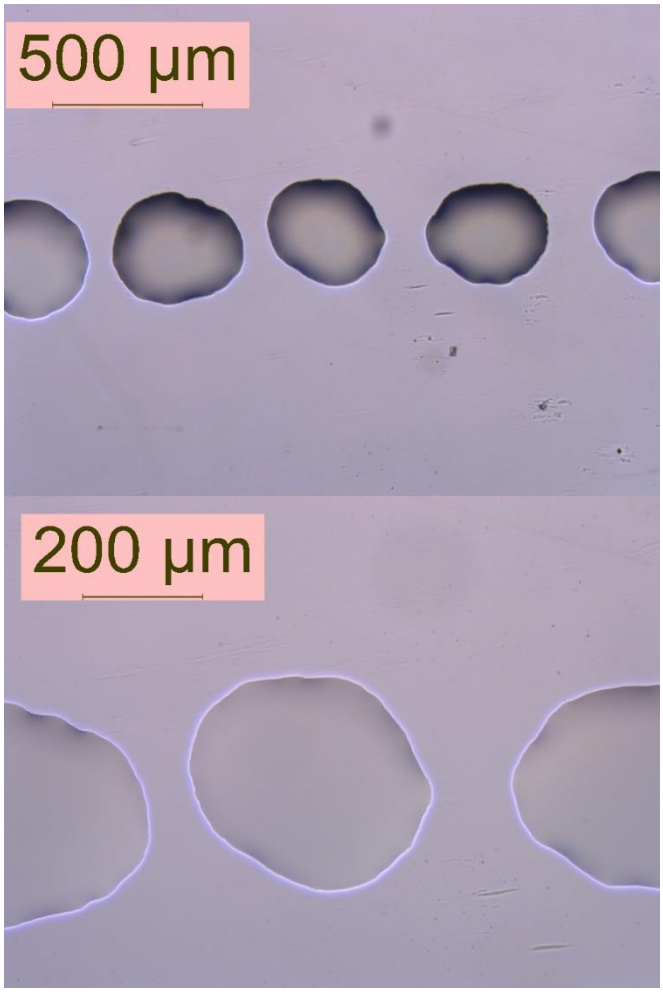

Figure 49: Bioink transferred on the substrate with 0.66 graphene EAL and 30μJ laser pulse energy

With 0.66μm graphene EAL and 30μJ laser pulse energy, the droplets deposited on the substrate were evenly distributed with 500μm gaps in between. All droplets were in irregular round shape. The diameter of the droplet was about 440μm.

Group12: 0.66 graphene EAL and 40μJ laser pulse energy

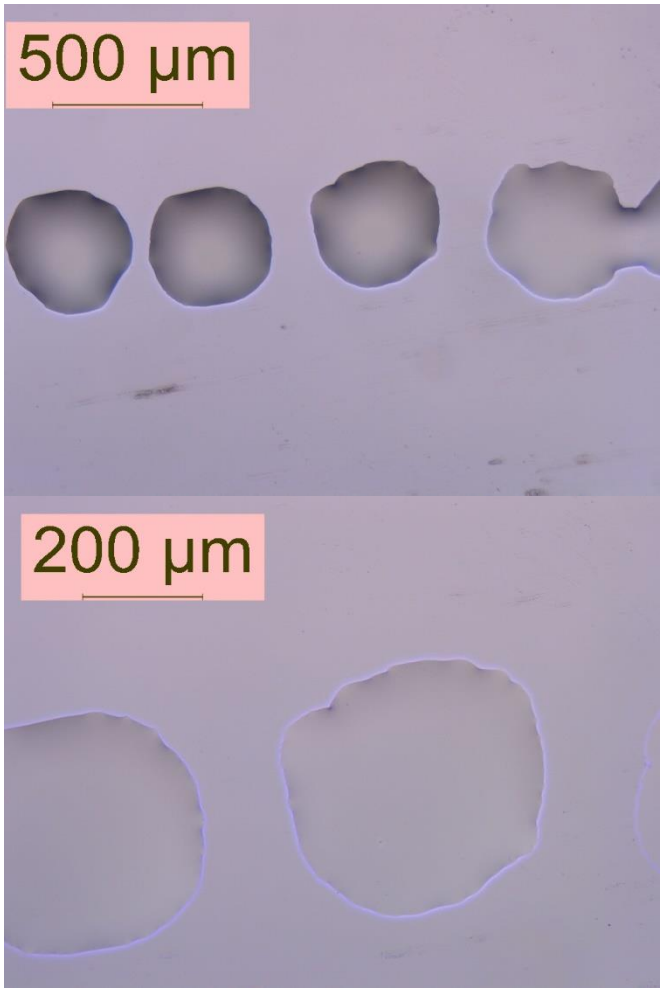

Figure 50: Bioink transferred on the substrate with 0.66 graphene EAL and 40μJ laser pulse energy

With 0.66μm graphene EAL and 40μJ laser pulse energy, the droplets deposited on the substrate were evenly distributed with 500μm gaps in between. Some droplets were in irregular round shape. Some of the droplets were connected. The diameter of the droplet was about 450μm.

Group13: 0.88 graphene EAL and 10μJ laser pulse energy

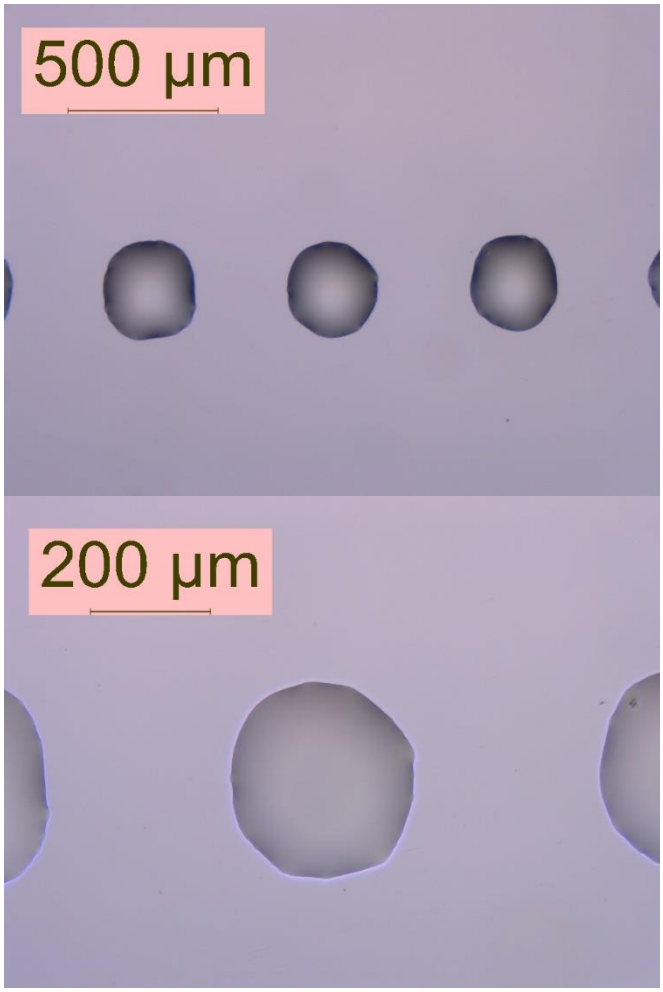

Figure 51: Bioink transferred on the substrate with 0.88 graphene EAL and 10μJ laser pulse energy

With 0.88μm graphene EAL and 10μJ laser pulse energy, the droplets deposited on the substrate were evenly distributed with 500μm gaps in between. All droplets were in regular round shape. The diameter of the droplet was about 310μm.

Group14: 0.88 graphene EAL and 20μJ laser pulse energy

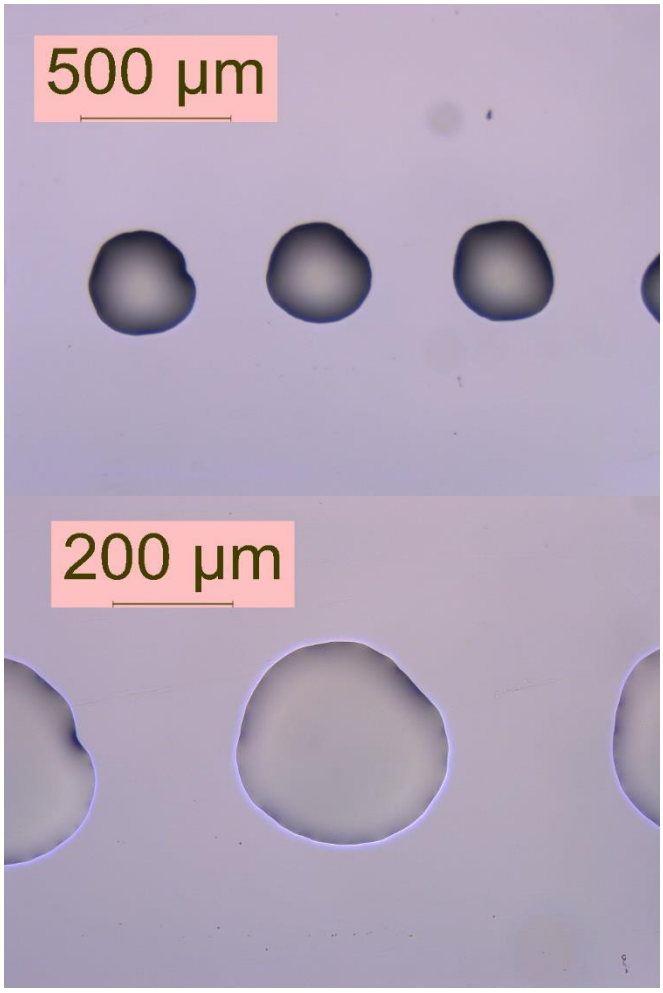

Figure 52: Bioink transferred on the substrate with 0.88 graphene EAL and 20μJ laser pulse energy

With 0.88μm graphene EAL and 20μJ laser pulse energy, the droplets deposited on the substrate were evenly distributed with 500μm gaps in between. Some droplets were in irregular round shape. The diameter of the droplet was about 350μm.

Group15: 0.88 graphene EAL and 30μJ laser pulse energy

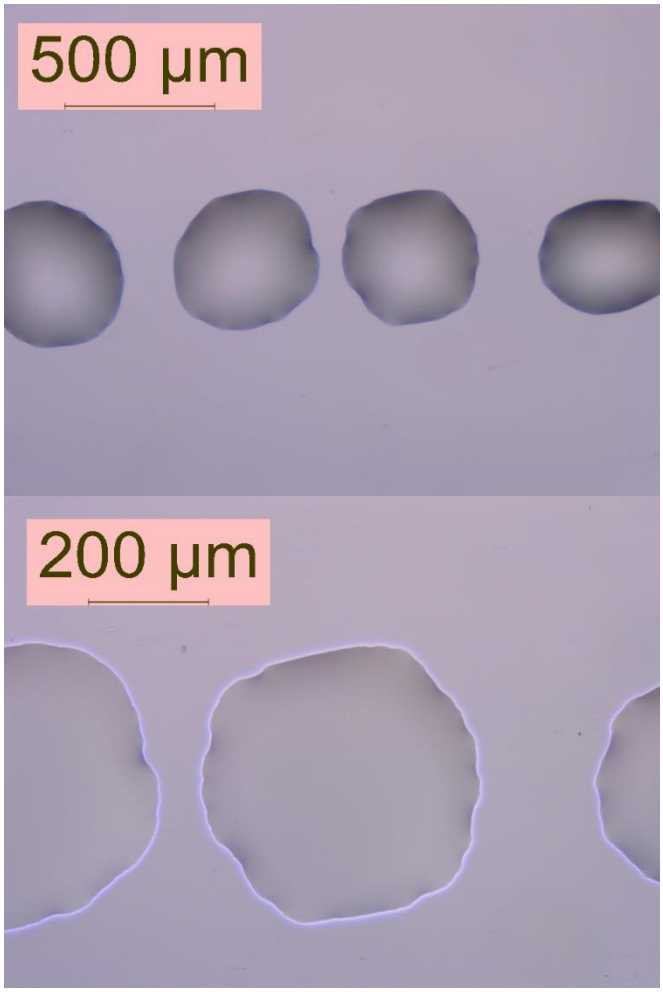

Figure 53: Bioink transferred on the substrate with 0.88 graphene EAL and 30μJ laser pulse energy

With 0.88μm graphene EAL and 30μJ laser pulse energy, the droplets deposited on the substrate were evenly distributed with 500μm gaps in between. Some droplets were in irregular round shape. The diameter of the droplet was about 460μm.

Group16: 0.88 graphene EAL and 40μJ laser pulse energy

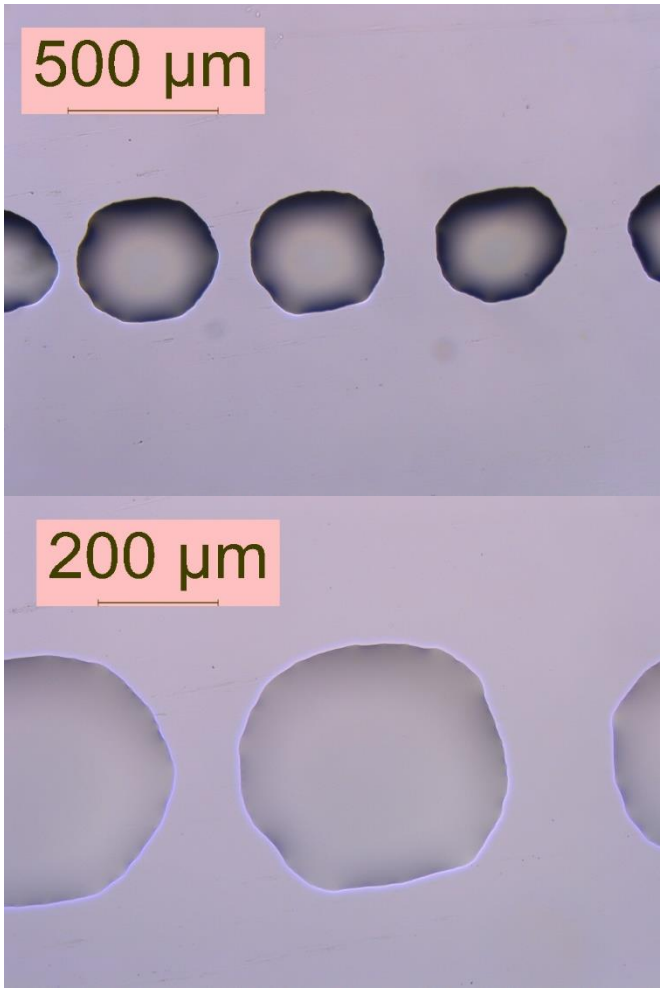

Figure 54: Bioink transferred on the substrate with 0.88 graphene EAL and 40μJ laser pulse energy

With 0.88μm graphene EAL and 40μJ laser pulse energy, the droplets deposited on the substrate were evenly distributed with 500μm gaps in between. Some droplets were in irregular round shape. The diameter of the droplet was about 450μm.

Group17: 1.10 graphene EAL and 10µJ laser pulse energy

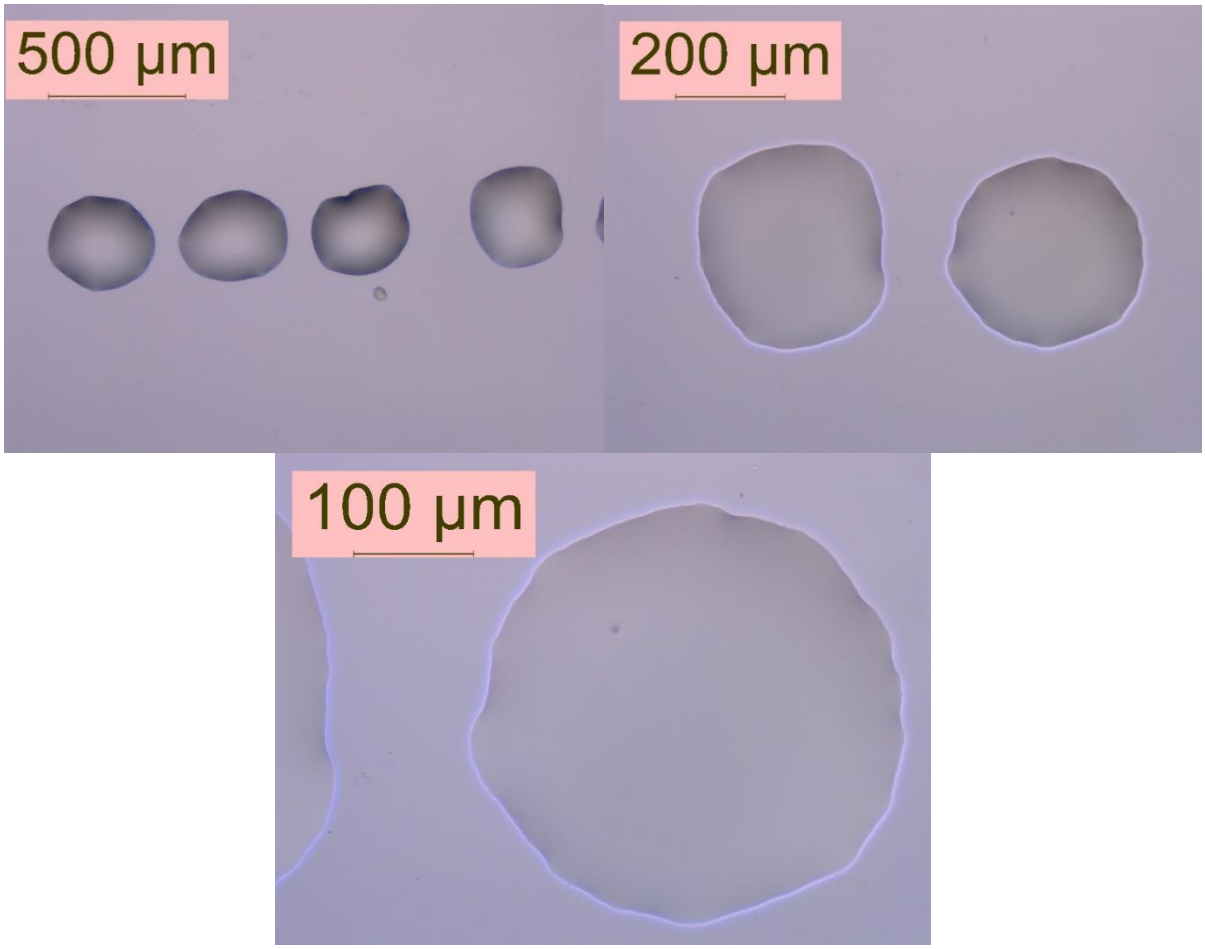

Figure 55: Bioink transferred on the substrate with 1.10 graphene EAL and 10µJ laser pulse energy

With 1.10µm graphene EAL and 10µJ laser pulse energy, the droplets deposited on the substrate were evenly distributed with 500µm gaps in between. All droplets were in irregular round shape. The diameter of the droplet was about 340µm.

Group18: 1.10 graphene EAL and 10µJ laser pulse energy

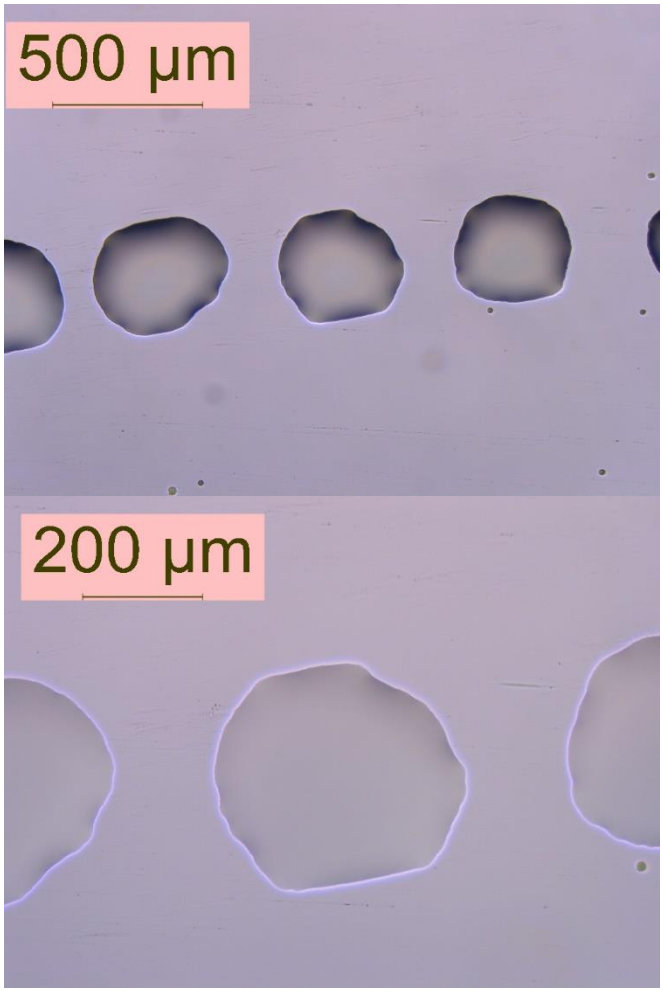

Figure 56: Bioink transferred on the substrate with 1.10 graphene EAL and 20µJ laser pulse energy

With 1.10µm graphene EAL and 20µJ laser pulse energy, the droplets deposited on the substrate were evenly distributed with 500µm gaps in between. All droplets were in irrgular round shape. The diameter of the droplet was about 400µm.

Group19: 1.10 graphene EAL and 30µJ laser pulse energy

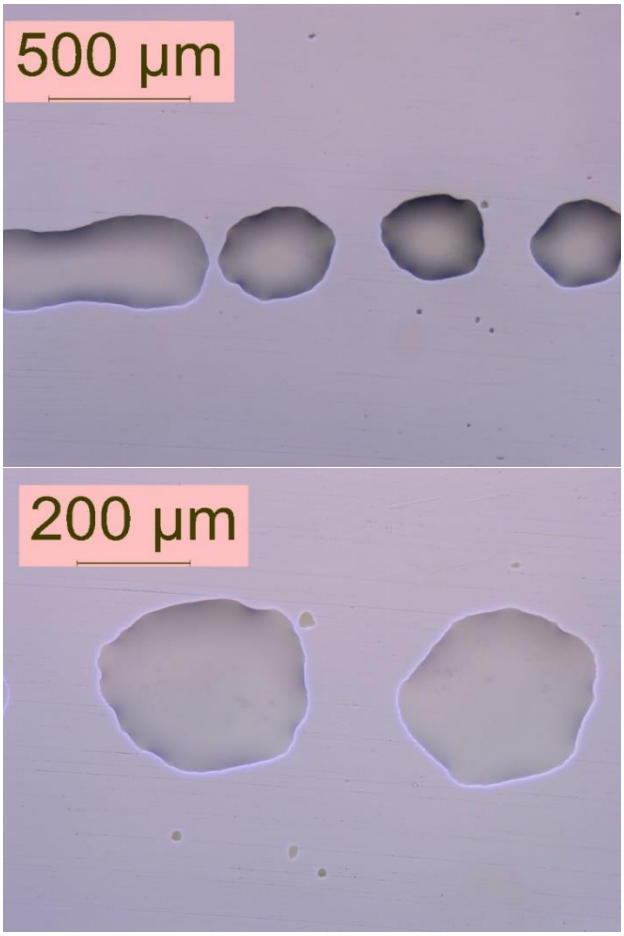

Figure 57: Bioink transferred on the substrate with 1.10 graphene EAL and 30µJ laser pulse energy

With 1.10µm graphene EAL and 30µJ laser pulse energy, the droplets deposited on the substrate were evenly distributed with 500µm gaps in between. All droplets were in irregular round shape. Some of the droplets were merged with adjacent droplet. The diameter of the droplet was about 350µm.

Group20: 1.10 graphene EAL and 40μJ laser pulse energy

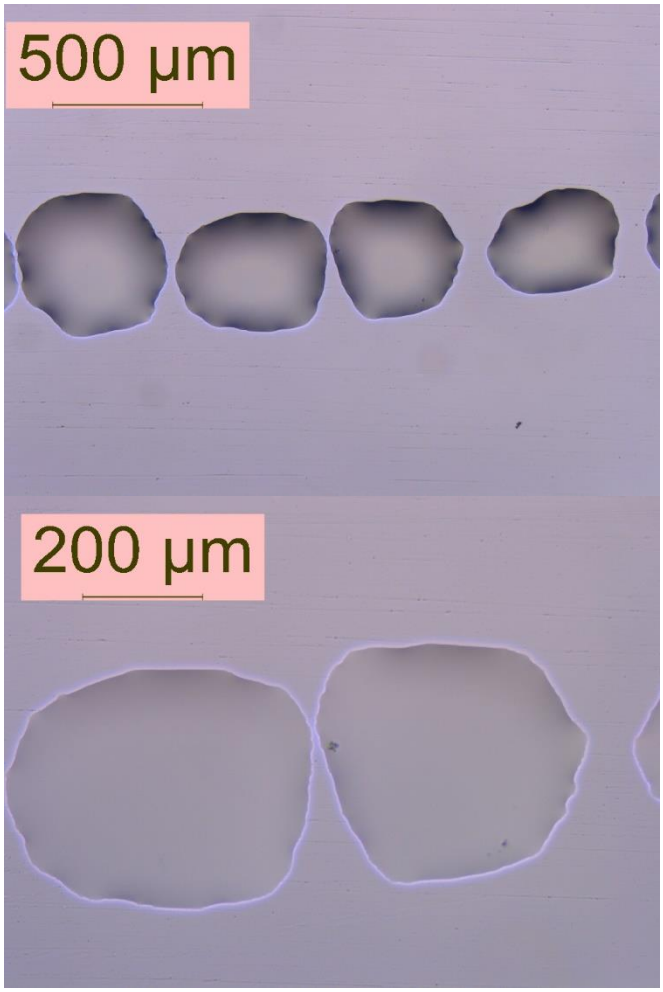

Figure 58: Bioink transferred on the substrate with 1.10 graphene EAL and 40μJ laser pulse energy

With 1.10 um graphene EAL and 40μJ laser pulse energy, the droplets deposited on the substrate were evenly distributed with 500μm gaps in between. All droplets were in irregular shape. The diameter of the droplet was about 450μm.

The diameters of the droplets transferred on the glass substrates are put together below list in the table 4.

Table 4: The droplet diameter with different laser pulse energy and EAL thickness

	10μJ	20μJ	30μJ	40μJ
0.22μm	300μm	340μm	400μm	440μm
0.44μm	340μm	400μm	450μm	490μm
0.66μm	350μm	420μm	440μm	450μm
0.88μm	310μm	350μm	460μm	450μm
1.1μm	340μm	400μm	350μm	450μm

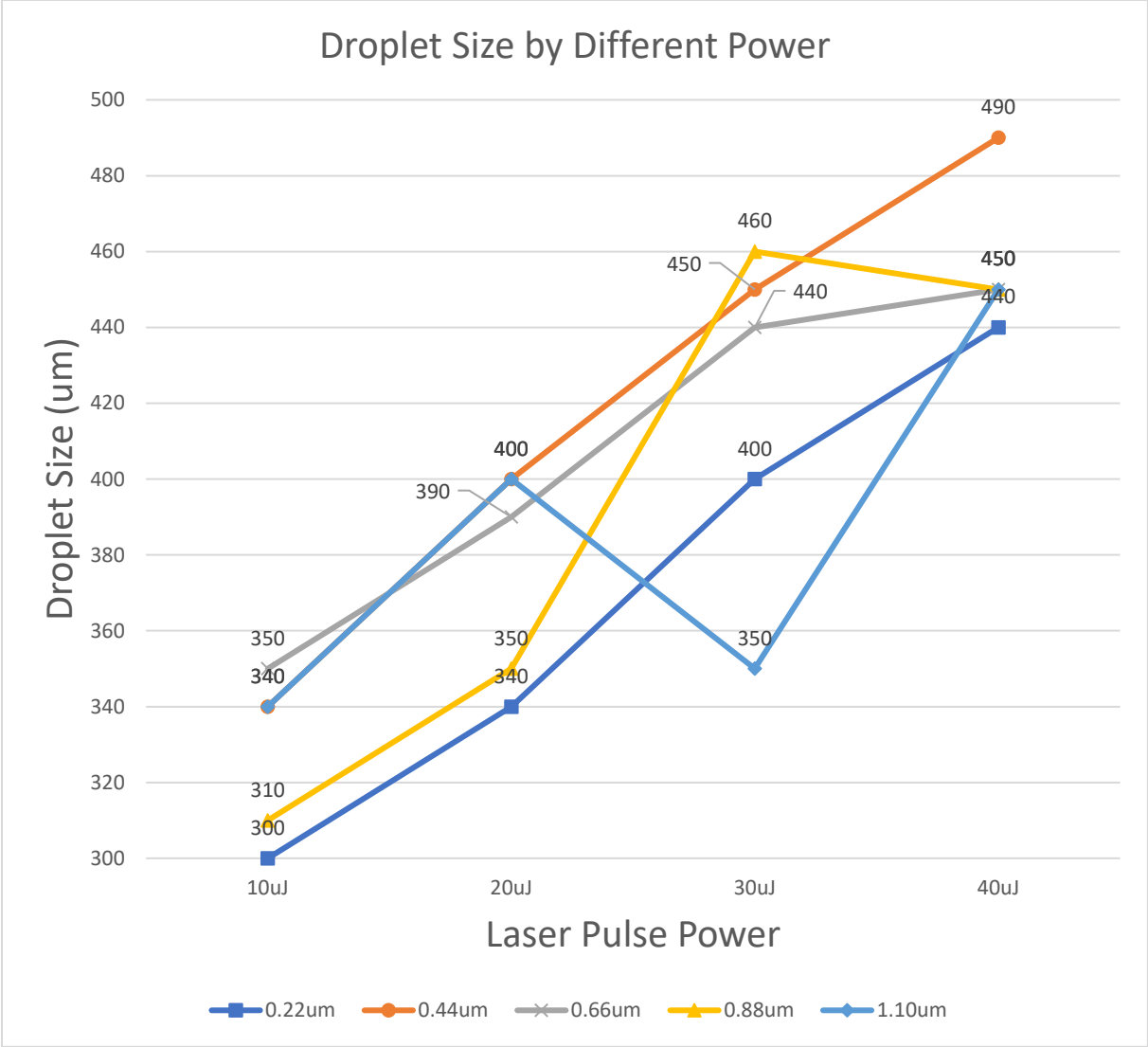

Figure 59: Droplet size by different power

It can be concluded from the Figure 59 that the droplet size is liner proportional to the laser pulse energy with the scope about 5μm/μJ, which means with every 1μJ increase in the laser pulse energy, the droplet size will increase 5μm.

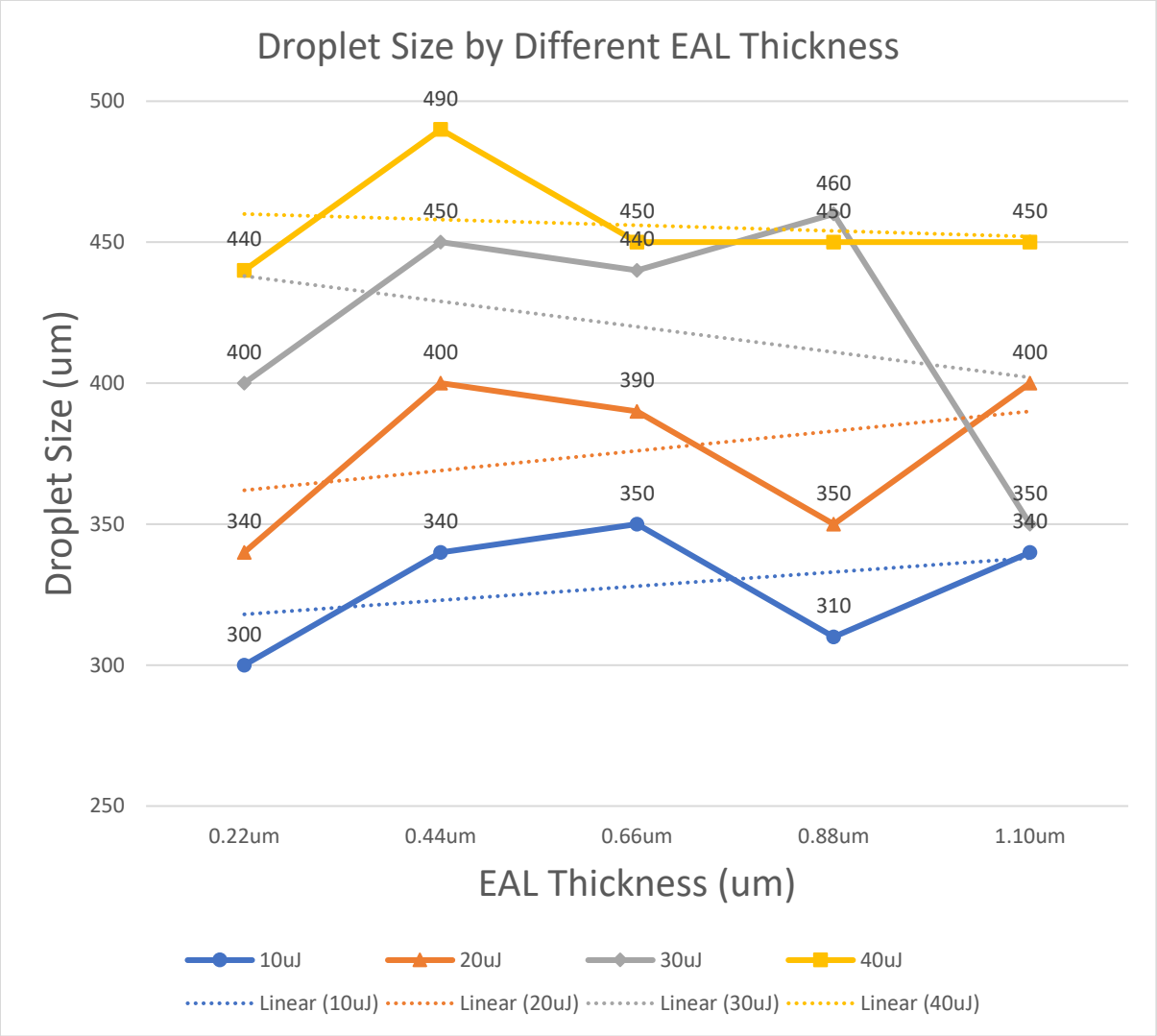

Figure 60: Droplet size by different EAL thickness

It can be seen from the Figure 60 that when the laser pulse energy is low (10μJ and 20μJ), the droplet size becomes larger when the EAL thickness becomes larger. When the laser pulse energy is high (30μJ and 40μJ), the droplet size becomes smaller when the EAL thickness becomes larger. However, all the changes in droplet size by different EAL thickness are in a small range. The conclusion can be made that the droplet size is not sensitive to the EAL thickness in this study.

4.3 Conclusion

4.3.1 The vaporization of the EAL

For the LAB process, the laser is the only energy source. Under this circumstance, the importance of the medium to convert the laser energy to the thermal energy and the kinetic energy is highlighted. There are two different setups of LAB corresponding to two different energy convert method. The LIFT uses an energy absorbing layer to absorb the laser and convert it to the transfer of the bioink. The other setup called MAPLE-DW, which directly utilizes the bioink as the laser absorbing medium.

The EAL is a specially designed layer attached to the bottom side of the ribbon. This layer is aimed at absorbing the laser light energy and generate a vapor bubble and further provide kinetic energy for bioink to be transferred. Traditionally, the material of EAL is metal such as gold or titanium, metal oxides such as titanium oxide and polymer. All those materials are not transparent and have a very short penetration depth to light. The thickness of the metal EAL and metal oxide EAL are usually tens of nanometers, and the thickness of the polymer EAL is around 500-1000 nm. However, during the printing process, the laser will break the EAL and produce a lot of fragments. The nano or micro EAL fragments will contaminate the bioink and damage the cells. There is a potential solution to address this situation that uses a biocompatible material to build EAL. One promising material is the graphene and this material is tested in this study. The graphene has a black color which gives it the great ability of laser absorption. The biocompatibility of the graphene may reduce the damage to the biomaterial.

The photos taken by the microscope clearly shows that at the focal point, the graphene EAL is removed by the laser pulse and the removal area is circular shape. The laser energy

confirms to Gaussian distribution, which means there is more energy concentrate to the center of the light spot. It can be seen from Figure 28, 29, 30, and 31 that with the increase of the laser pulse energy, the affected zone on the graphene EAL is getting larger. As on the 0.88μm graphene EAL, the 10μJ laser pulse removed a circular area with the diameter of 75μm; the 20μJ laser pulse removed a circular area with the diameter of 100μm; the 10μJ laser pulse removed a circular area with the diameter of 120μm; the 10μJ laser pulse removed a circular area with the diameter of 135μm.

From the data above, we can draw the conclusion that with the increase of the laser energy, the affected zone on the EAL is, almost linearly, getting larger. This may be caused by the increased laser fluence that makes the Gaussian spot contains a higher energy level and expand the area to pass the energy threshold of graphene removal. The diameter of the EAL affected zone is liner proportional to the laser pulse energy in the range from 10μJ to 40μJ with a scope 1.5μm/μJ, which means by 1μJ increase in the laser pulse energy will cause 1.5μm increase in the Affected zone diameter.

4.3.2 Droplet size

The droplet size on the substrate is one of the most important indices to assess the printing result. The droplet was created by the jet which brings the bioink from the ribbon to the substrate. The size and the speed of the jet determine the diameters of the droplets. If the jet is stronger and faster, there will be more bioink transferred, and the size of the droplet will be larger.

From the data above, it can be concluded that the droplet size becomes larger as the laser pulse energy goes higher. This is because the higher energy one laser pulse has, the more is

absorbed by the graphene EAL. The bubble generated in the bioink layer grows faster and larger which will push more bioink that transferred to the substrate via the jet. It can be concluded from the figure 59 that the droplet size is liner proportional to the laser pulse energy with a scope about 5μm/μJ, which means 1μJ increase in the laser pulse energy will increase the droplet diameter by 5μm.

As shown in the figure 60, the graphene EAL thickness has less effect on the droplet size than laser pulse energy. The thicker the graphene EAL, the less transparency the EAL has, and more laser energy should be absorbed. However, at the same time, thicker EAL means more energy will be consumed to vaporize the EAL and a smaller bubble/jet will appear. These two factors cancel each other. From the experiments in this thesis, with different EAL thicknesses, the droplets have similar diameters with different laser pulse energy.

4.3.3 Fully develop of the jet

The distance between the ribbon and the substrate is named the travel distance. This distance has a very strong relation with the bioink transfer. If the distance is too small, the jet is not formed completely. If the distance is too large, the jet will break or retract before touching the substrate. Both situations are not good for bioprinting. In this study, the gap between the ribbon and the substrate is 500μm. The first jets of all groups with 0.22μm graphene EAL are all fully developed. The following bioink transfer is through the initial jet.

CHAPTER V

SUMMARY AND FUTURE WORK

5.1 Overview

With the development of additive manufacturing, the laser assisted bioprinting is innovated as an advanced biomanufacturing method. Even though researchers made a lot of progress in this realm, there is still a long way to achieve tissue/organ printing which can be used in real medical cases such as organ transplantation or personalized drug design/development. For more than a decade, in the LAB printing, the stabilizing of the droplet, the optimization of the accuracy and the enhancement of the cell viability became the key research topics.

The original plan of this study was to test the printability of water-based graphene solution and the performance of graphene energy absorbing layer. The experimental results confirmed to some degree that the graphene EAL can indeed enhance laser absorbing rate and helped the generation of bubble/jet. It can be stated that the performance of the LAB printing basically relied on three factors:

- Laser pulse energy;
- Bioink layer thickness;
- Bioink properties.

In general, the achievement of this research can be concluded as follows:

1. Designed and established the bioprinting environment;
2. Tested the performance of graphene energy absorbing layer;
3. Record different bubble/jet formation process.

The innovations put forward by this thesis are as following:

1. Invented a novel coating strategy for low viscous bioink.

A volume-based coating method is put forward to achieve a uniform bioink layer. Due to the difficulty of coating, the low viscosity bioink on the glass slide, the spin coating and the blade coating is hard to achieve a thin and uniform bioink layer on the ribbon and the thickness of the bioink layer cannot be controlled accurately. The coating method used in this thesis is based on the volume of the bioink layer. By controlling the coating area, the thickness of the bioink layer is easily be controlled with a minor error.

2. Innovative use of graphene as the energy absorbing layer

Different from wildly used metal EAL or metal oxide EAL, the graphene EAL does not need a plasma coating machine which makes the ribbon much easier to prepare. The graphene water dispersion is used to deposit the graphene layer on the ribbon. By using the pipette to transfer the calculated amount of graphene dispersion on the slide and pave the liquid, a uniform absorbing layer can be prepared.

5.2 Additional challenges

The graphene EAL has demonstrated laser absorbing performance in the LAB printer with femtosecond infrared laser and the bioink is successfully transferred to the substrate at the correct location. However, there are still some unstudied problems left that are related to the laser assisted bioprinting. That include four major ones:

- Study how the graphene fragments affect the bioink and the cells
- Record the printing process with more details and higher frame rate
- Explore a better method to coat EAL
- Printing of non-regular shape cells

By using the volume-based coating method, a uniform EAL and bioink layer can be prepared with accurate thickness. However, the bioink layer is still uneven at a smaller thickness. When a liquid layer equal or under 50μm is applied, the layer is hard to be equalized in thickness. A new coating method should be explored to address this problem.

The high-speed camera used in this thesis to observe the bubble jet formation is Evo 410L which can take 57000 frames per second at the resolution of 256*256 pixels. However, the bubble/ jet formation process is so fast that the time scale is beyond the ability of the high-speed camera used in this study. To observe this process in a more detailed view, a powerful camera is needed to be the recorder.

Furthermore, the lens used in the experiment is a modular lens from Navitar, which can achieve around 1μm per pixel in maximum when cooperating with the camera. If further study regarding the bubble/jet formation is needed, a lens with higher magnification will be required.

The bioink tested in this thesis is 67% water-glycerol solution. The cell has not been applied in this study. In the practical bioprinting, the cell is the most essential part of the bioink. The purpose of testing graphene is to find a better EAL material that can avoid the contamination of bioink and the damage of cells. The performance of this material as EAL is tested and it has been proved as a good laser absorbing material. However, cell viability is not tested in the experiment. It is not clear that the graphene will enhance the viability of the cell or damage the cell under the circumstance of LAB. The influence of the graphene fragments to bioink and cells still needs to be explored.

Moreover, new EAL material should be tested. Researchers have already claimed may promising materials like polymers, ceramic, and hydrogel. Many performances of the EAL has the potential to be improved such as a non-broken EAL will improve the printing efficiency and the cell viability, bio-absorbing material can reduce the EAL fragments in the bioink and enhance the cell survival rate.

Printing of non-regular shaped cells or non-spherical cells is an important topic of LAB. Up to now, the LAB printing method can only process regular round shape cells and has not been tested with non-regular cells. However, in real cases, different cells have different shapes, and many of them are not regular spherical shape. For instance, nerve cells are in long shape; the erythrocytes look like disks. To realize the goal of tissue printing, a method to control the morphology of the bubble and jet is required to process different shapes of cells. Among all different bioprinting technology, the LAB is the most unique one since it does not have a nozzle structure, which gives it the great ability to manipulate single cells with higher freedom than other methods. By studying the bubble/jet formation process and the printing parameters, the printing of non-regular cells will be achieved.

REFERENCES

Barron JA, Ringeisen BR, Kim H, Spargo BJ, Chrisey DB (2004a) Application of laser printing to mammalian cells. Thin Solid Films 453-454:383-387. doi:10.1016/j.tsf.2003.11.161

Barron JA, Spargo BJ, Ringeisen BR (2004b) Biological laser printing of three dimensional cellular structures. Applied Physics A 79 (4-6):1027-1030. doi:10.1007/s00339-004-2620-3

Barron JA, Wu P, Ladouceur HD, Ringeisen BR (2004c) Biological Laser Printing: A Novel Technique for Creating Heterogeneous 3-dimensional Cell Patterns. Biomedical Microdevices 6 (2):139-147. doi:10.1023/B:BMMD.0000031751.67267.9f

Bohandy J, Kim BF, Adrian FJ (1986) Metal deposition from a supported metal film using an excimer laser. Journal of Applied Physics 60 (4):1538-1539. doi:10.1063/1.337287

Brown MS, Kattamis NT, Arnold CB (2010) Time-resolved study of polyimide absorption layers for blister-actuated laser-induced forward transfer. Journal of Applied Physics 107 (8):083103. doi:10.1063/1.3327432

Catros S, Fricain JC, Guillotin B, Pippenger B, Bareille R, Remy M, Lebraud E, Desbat B, Amedee J, Guillemot F (2011) Laser-assisted bioprinting for creating on-demand patterns of human osteoprogenitor cells and nano-hydroxyapatite. Biofabrication 3 (2):025001. doi:10.1088/1758-5082/3/2/025001

Chen CY, Barron JA, Ringeisen BR (2006) Cell patterning without chemical surface modification: Cell–cell interactions between printed bovine aortic endothelial cells (BAEC) on a homogeneous cell-adherent hydrogel. Applied Surface Science 252 (24):8641-8645. doi:10.1016/j.apsusc.2005.11.088

Deng Y, Renaud P, Guo Z, Huang Z, Chen Y (2017) Single cell isolation process with laser induced forward transfer. J Biol Eng 11:2. doi:10.1186/s13036-016-0045-0

Dinca V, Farsari M, Kafetzopoulos D, Popescu A, Dinescu M, Fotakis C (2008) Patterning parameters for biomolecules microarrays constructed with nanosecond and femtosecond UV lasers. Thin Solid Films 516 (18):6504-6511. doi:10.1016/j.tsf.2008.02.043

Doraiswamy A, Narayan RJ, Lippert T, Urech L, Wokaun A, Nagel M, Hopp B, Dinescu M, Modi R, Auyeung RCY, Chrisey DB (2006) Excimer laser forward transfer of mammalian cells using a novel triazene absorbing layer. Applied Surface Science 252 (13):4743-4747. doi:10.1016/j.apsusc.2005.07.166

Duocastella M, Fernández-Pradas JM, Morenza JL, Serra P (2009) Time-resolved imaging of the laser forward transfer of liquids. Journal of applied physics. Journal of applied physics 106 (8):084907. doi:10.1063/1.3248304

Duocastella M, Fernández-Pradas JM, Morenza JL, Zafra D, Serra P (2010a) Novel laser printing technique for miniaturized biosensors preparation. Sensors and Actuators B: Chemical 145 (1):596-600. doi:10.1016/j.snb.2009.11.055

Duocastella M, Fernández-Pradas JM, Serra JLMP (2010b) Sessile droplet formation in the laser-induced forward transfer of liquids: A time-resolved imaging study. Thin Solid Films 518 (18):5321-5325. doi:10.1016/j.tsf.2010.03.082

Duocastella M, Fernández-Pradas JM, Serra P, Morenza JL (2008) Jet formation in the laser forward transfer of liquids. Applied Physics A 93 (2):453-456. doi:10.1007/s00339-008-4781-y

Fernández-Pradas JM, Colina M, Serra P, Domínguez J, Morenza JL (2004) Laser-induced forward transfer of biomolecules. Thin Solid Films 453-454:27-30. doi:10.1016/j.tsf.2003.11.154

Fernández-Pradas JM, Rodríguez-Vázquez Á, Duocastella M, Colina M, Liñán-Cembrano G, Serra P, Morenza JL (2007) Production of miniaturized biosensors through laser-induced forward transfer. Paper presented at the Bioengineered and Bioinspired Systems III,

Gruene M, Deiwick A, Koch L, Schlie S, Unger C, Hofmann N, Bernemann I, Glasmacher B, Chichkov B (2011a) Laser printing of stem cells for biofabrication of scaffold-free autologous grafts. Tissue Eng Part C Methods 17 (1):79-87. doi:10.1089/ten.TEC.2010.0359

Gruene M, Unger C, Koch L, Deiwick A, Chichkov B (2011b) Dispensing pico to nanolitre of a natural hydrogel by laser-assisted bioprinting. BioMedical Engineering OnLine 10 (1):19. doi:10.1186/1475-925X-10-19

Gudapati H, Yan J, Huang Y, Chrisey DB (2014) Alginate gelation-induced cell death during laser-assisted cell printing. Biofabrication 6 (3):035022. doi:10.1088/1758-5082/6/3/035022

Guillemot F, Souquet A, Catros S, Guillotin B (2010a) Laser-assisted cell printing: principle, physical parameters versus cell fate and perspectives in tissue engineering. Nanomedicine 5 (3):507-515

Guillemot F, Souquet A, Catros S, Guillotin B, Lopez J, Faucon M, Pippenger B, Bareille R, Remy M, Bellance S, Chabassier P, Fricain JC, Amedee J (2010b) High-throughput laser printing of cells and biomaterials for tissue engineering. Acta Biomater 6 (7):2494-2500. doi:10.1016/j.actbio.2009.09.029

Guillotin B, Ali M, Ducom A, Catros S, Keriquel V, Souquet A, Remy M, Fricain J-C, Guillemot F (2013) Laser-Assisted Bioprinting for Tissue Engineering. In: Biofabrication. pp 95-118. doi:10.1016/b978-1-4557-2852-7.00006-8

Guillotin B, Souquet A, Catros S, Duocastella M, Pippenger B, Bellance S, Bareille R, Remy M, Bordenave L, Amedee J, Guillemot F (2010) Laser assisted bioprinting of engineered tissue with high cell density and microscale organization. Biomaterials 31 (28):7250-7256. doi:10.1016/j.biomaterials.2010.05.055

Haider AJ, Haider MJ, Majed MD, Mohammed AH, Mansour HL (2017) Effect of Laser Fluence on a Microarray Droplets Micro-Organisms Cells by LIFT Technique. Energy Procedia 119:256-263. doi:https://doi.org/10.1016/j.egypro.2017.07.078

Hopp B, Smausz T, Antal Z, Kresz N, Bor Z, Chrisey D (2004) Absorbing film assisted laser induced forward transfer of fungi. Journal of applied physics 96 (6):3478-3481

Hopp B, Smausz T, Kresz N, Barna N, Bor Z, Kolozsvári L, Chrisey DB, Szabó A, Nógrádi A (2005) Survival and Proliferative Ability of Various Living Cell Types after Laser-Induced Forward Transfer. Tissue Engineering 11 (11-12):1817-1823. doi:10.1089/ten.2005.11.1817

Hopp B, Smausz T, Nógrádi A (2010) Absorbing-Film Assisted Laser Induced Forward Transfer of Sensitive Biological Subjects. In: Ringeisen BR, Spargo BJ, Wu PK (eds) Cell and

Organ Printing. Springer Netherlands, Dordrecht, pp 115-134. doi:10.1007/978-90-481-9145-1_7

Karaiskou A, Zergioti I, Fotakis C, Kapsetaki M, Kafetzopoulos D (2003) Microfabrication of biomaterials by the sub-ps laser-induced forward transfer process. Applied Surface Science 208-209:245-249. doi:10.1016/s0169-4332(02)01396-x

Kennedy PK, Boppart SA, Hammer DX, Rockwell BA, Noojin GD, Roach WP (1995) A first-order model for computation of laser-induced breakdown thresholds in ocular and aqueous media. II. Comparison to experiment. IEEE Journal of Quantum Electronics 31 (12):2250-2257. doi:10.1109/3.477754

Keriquel V, Oliveira H, Remy M, Ziane S, Delmond S, Rousseau B, Rey S, Catros S, Amedee J, Guillemot F, Fricain JC (2017) In situ printing of mesenchymal stromal cells, by laser-assisted bioprinting, for in vivo bone regeneration applications. Sci Rep 7 (1):1778. doi:10.1038/s41598-017-01914-x

Kerouredan O, Bourget JM, Remy M, Crauste-Manciet S, Kalisky J, Catros S, Thebaud NB, Devillard R (2019) Micropatterning of endothelial cells to create a capillary-like network with defined architecture by laser-assisted bioprinting. J Mater Sci Mater Med 30 (2):28. doi:10.1007/s10856-019-6230-1

Koch L, Deiwick A, Chichkov B (2014) Laser-based 3D cell printing for tissue engineering. BioNanoMaterials 15 (3-4). doi:10.1515/bnm-2014-0005

Koch L, Deiwick A, Franke A, Schwanke K, Haverich A, Zweigerdt R, Chichkov B (2018) Laser bioprinting of human induced pluripotent stem cells-the effect of printing and

biomaterials on cell survival, pluripotency, and differentiation. Biofabrication 10 (3):035005. doi:10.1088/1758-5090/aab981

Lin Y, Huang Y, Chrisey DB (2009) Droplet formation in matrix-assisted pulsed-laser evaporation direct writing of glycerol-water solution. Journal of Applied Physics 105 (9). doi:10.1063/1.3116724

Lin Y, Huang Y, Chrisey DB (2011) Metallic Foil-Assisted Laser Cell Printing. Journal of Biomechanical Engineering 133 (2). doi:10.1115/1.4003132

Mezel C, Souquet A, Hallo L, Guillemot F (2010) Bioprinting by laser-induced forward transfer for tissue engineering applications: jet formation modeling. Biofabrication 2 (1):014103. doi:10.1088/1758-5082/2/1/014103

Nguyen AK, Narayan RJ (2017) Liquid-Phase Laser Induced Forward Transfer for Complex Organic Inks and Tissue Engineering. Ann Biomed Eng 45 (1):84-99. doi:10.1007/s10439-016-1617-3

Othon CM, Wu X, Anders JJ, Ringeisen BR (2008) Single-cell printing to form three-dimensional lines of olfactory ensheathing cells. Biomed Mater 3 (3):034101. doi:10.1088/1748-6041/3/3/034101

Ringeisen BR, Rincon K, Fitzgerald LA, Fulmer PA, Wu PK, Gilbert M (2014) Printing soil: a single-step, high-throughput method to isolate micro-organisms and near-neighbour microbial consortia from a complex environmental sample. Methods in Ecology and Evolution 6 (2):209-217. doi:10.1111/2041-210x.12303

Serra P, Duocastella M, Fernández-Pradas JM, Morenza JL (2009) Liquids microprinting through laser-induced forward transfer. Applied Surface Science 255 (10):5342-5345. doi:10.1016/j.apsusc.2008.07.200

Serra P, Piqué A (2019) Laser-Induced Forward Transfer: Fundamentals and Applications. Advanced Materials Technologies 4 (1). doi:10.1002/admt.201800099

Smausz T, Hopp B, Kecskeméti G, Bor Z (2006) Study on metal microparticle content of the material transferred with Absorbing Film Assisted Laser Induced Forward Transfer when using silver absorbing layer. Applied Surface Science 252 (13):4738-4742. doi:10.1016/j.apsusc.2005.07.115

Unger C, Gruene M, Koch L, Koch J, Chichkov BN (2010) Time-resolved imaging of hydrogel printing via laser-induced forward transfer. Applied Physics A 103 (2):271-277. doi:10.1007/s00339-010-6030-4

Vogel A, Noack J, Nahen K, Theisen D, Busch S, Parlitz U, Hammer DX, Noojin GD, Rockwell BA, Birngruber R (1999) Energy balance of optical breakdown in water at nanosecond to femtosecond time scales. Applied Physics B 68 (2):271-280. doi:10.1007/s003400050617

Wang W, Li G, Huang Y (2009) Modeling of Bubble Expansion-Induced Cell Mechanical Profile in Laser-Assisted Cell Direct Writing. Journal of Manufacturing Science and Engineering 131 (5). doi:10.1115/1.4000101

Xiong R, Zhang Z, Chai W, Chrisey DB, Huang Y (2017) Study of gelatin as an effective energy absorbing layer for laser bioprinting. Biofabrication 9 (2):024103. doi:10.1088/1758-5090/aa74f2

Xiong R, Zhang Z, Shen J, Lin Y, Huang Y, Chrisey DB (2015) Bubble Formation Modeling During Laser Direct Writing of Glycerol Solutions. Journal of Micro and Nano-Manufacturing 3 (1). doi:10.1115/1.4029264

Yan J, Huang Y, Chrisey DB (2013) Laser-assisted printing of alginate long tubes and annular constructs. Biofabrication 5 (1):015002. doi:10.1088/1758-5082/5/1/015002

Zergioti I, Karaiskou A, Papazoglou DG, Fotakis C, Kapsetaki M, Kafetzopoulos D (2005) Time resolved schlieren study of sub-pecosecond and nanosecond laser transfer of biomaterials. Applied Surface Science 247 (1-4):584-589. doi:10.1016/j.apsusc.2005.01.127

Zhang Z, Xiong R, Corr DT, Huang Y (2016) Study of Impingement Types and Printing Quality during Laser Printing of Viscoelastic Alginate Solutions. Langmuir 32 (12):3004-3014. doi:10.1021/acs.langmuir.6b00220

Zhang Z, Xu C, Xiong R, Chrisey DB, Huang Y (2017) Effects of living cells on the bioink printability during laser printing. Biomicrofluidics 11 (3):034120. doi:10.1063/1.4985652

APPENDIX

APPENDIX

CODE FOR EXPERIMENTS

```
DVAR $XC $YC $ZC

$XC=-11.85
$YC=74.15
$ZC=111.2

enable X Y Z

home X Y Z

SCOPETRIG

ABSOLUTE

f 10

PSOCONTROL Z RESET
```

```
PSOOUTPUT Z CONTROL 0 1

$AO[0].Z = 1.25

G0 X $XC Y 72

G0 Y $YC Z $ZC

PSOCONTROL Z ON

 G1 Y $YC-10 Z $ZC

 G1 X $XC+0.3 Z $ZC

 G1 Y $YC Z $ZC

 G1 X $XC+0.6 Z $ZC

 G1 Y $YC-10 Z $ZC

 G1 X $XC+0.9 Z $ZC

 G1 Y $YC Z $ZC
```

G1 X $XC+1.2 Z $ZC

G1 Y $YC-10 Z $ZC

G1 X $XC+1.5 Z $ZC

G1 Y $YC Z $ZC

G1 X $XC+1.8 Z $ZC

G1 Y $YC-10 Z $ZC

G1 X $XC+2.1 Z $ZC

G1 Y $YC Z $ZC

G1 X $XC+2.4 Z $ZC

G1 Y $YC-10 Z $ZC

G1 X $XC+2.7 Z $ZC

```
 G1 Y $YC Z $ZC

 G1 X $XC+3 Z $ZC

PSOCONTROL Z OFF

$AO[0].Z = 0

END program
```

BIOGRAPHICAL SKETCH

Graduated in 2015 from the Southeast University Chengxian College with a Bachelor of Science in Mechanical Engineering. Received a Master of Science in Mechanical Engineering from Yangzhou University. Entered a Master of Science in Manufacturing Engineering program at University of Texas Rio Grande Valley in 2018 and graduating in Aug 2020.

Email: chaorandou@hotmail.com